Electronic Structure and Bonding in Monocarbonyl Adducts of Dimolybdenum and Ditungsten Hexaalkoxides: A Theoretical and Spectroscopic Investigation into the Mechanism of M–M and C–O Bond Order Reduction

P. J. Blower, M. H. Chisholm,* D. L. Clark, and B. W. Eichhorn

Department of Chemistry, Indiana University, Bloomington, Indiana 47405

Received January 13, 1986

The reaction between CO and the M≡M bonded compounds $M_2(OR)_6$ (M = Mo or W) can yield both dinuclear and tetranuclear products. The reaction sequence $W{\equiv}W + C{\equiv}O \rightarrow W_2(\mu\text{-}CO) \rightarrow [W_2(\mu\text{-}CO)]_2$ represents a stepwise reduction in M–M and C–O bond order from 3 to 2 to 1 [*Organometallics* **1985**, *4*, 986]. We have investigated the nature of CO reduction by the dimetal centers with the aid of nonparameterized Fenske–Hall calculations on the model systems $M_2(OH)_6(\mu\text{-}CO)$ and $M_2(OH)_6(NH_3)_2(\mu\text{-}CO)$, where M = Mo and W, as well as the tetranuclear compound $[W_2(OH)_6(\mu\text{-}CO)]_2$. Reduction of CO in these species takes place via a "power" back-bonding mechanism and the Mulliken populations of the canonical orbitals of the CO moiety can be used as a measure of the degree of CO reduction. The CO stretching frequencies, and hence the degree of CO reduction, correlate with the calculated occupancies of the CO 5σ and 2π orbitals. The differences in the binding of CO to the $(W{\equiv}W)^{6+}$ and $(Mo{\equiv}Mo)^{6+}$ units in $M_2(OR)_6$ compounds are related to the greater reducing power (π back-bonding) of the W_2^{6+} center relative to the Mo_2^{6+} center. Further reduction of CO requires the cooperative effects of two W_2 units, and electrochemically the $[W_2(\mu\text{-}CO)]_2$ species can be reduced even further. This reduction of CO bond order from 3 to 2 to 1 is suggestive of a model for the reaction pathway of CO on a metal oxide surface leading ultimately to carbide C^{4-} and oxide O^{2-}, and the prospects for the ultimate cleavage of the CO bond in these fascinating systems are discussed. UV–visible spectral data and electrochemical data are reported and compared with the results anticipated from the calculations.

Introduction

It has been known for some time that metal–metal bonds in reduced molybdenum and tungsten alkoxides provide a reservoir of electrons that may be used for single- or multi-electron reduction of small organic molecules.[1] Our advocation that reduced metal alkoxides may serve as hydrocarbon-soluble models for metal oxides is prompted by the recognition that metal oxides form an extremely important group of heterogeneous catalysts for activation of a wide variety of fundamentally important substrate molecules.[2] Reductive polymerization of carbon monoxide in Fischer–Tropsch chemistry is just one example where metal oxides are superior to homogeneous metal carbonyl compounds.[3] Thus, as part of our interest in developing the organometallic chemistry associated with M–M multiple bonds in metal alkoxides as models for metal oxides, we have been actively investigating the reactions between $M_2(OR)_6(M{\equiv}M)$ compounds (M = Mo, W) and carbon monoxide. We have shown that these reactions lead to cleavage of the M≡M bond and, by disproportionation, to $M(CO)_6$ and higher valent metal alkoxides.[4] The detailed course of the reaction depends intimately on the metal (Mo vs. W) and on the steric properties of the alkoxide ligands. In the case of $Mo_2(O\text{-}t\text{-}Bu)_6$, a stoichiometric reaction has been established and shown to proceed via the initial reversible formation of $Mo_2(O\text{-}t\text{-}Bu)_6(\mu\text{-}CO)$ which has the structure shown in I.

Table I. Pertinent Infrared and ^{13}C NMR Data for $W_2(\mu\text{-}CO)$ Containing Compounds

compd	$\nu(CO)$,[a] cm^{-1}	$\nu(^{13}CO)$, cm^{-1}	$\delta(^{13}CO)$[b]	ref
$Mo_2(O\text{-}t\text{-}Bu)_6(\mu\text{-}CO)$	1670	NR[d]	272.5	4
$W_2(O\text{-}t\text{-}Bu)_6(\mu\text{-}CO)$	1598	1559	291.0	7
	(1605)[c]			
$Mo_2(OCH_2\text{-}t\text{-}Bu)_6(py)_2(\mu\text{-}CO)$	1660	NR[d]	323.6	5
$W_2(OCH_2\text{-}t\text{-}Bu)_6(py)_2(\mu\text{-}CO)$	1587	1546	321.6	7
	1579	1538		
	1567			
	(1595)[c]	(1570)[c]		
$Mo_2(O\text{-}i\text{-}Pr)_6(py)_2(\mu\text{-}CO)$	1655	1618	331.5	5
$W_2(O\text{-}i\text{-}Pr)_6(py)_2(\mu\text{-}CO)$	1570		341[e]	7
	1579	1533		
	(1298)[c]	(1271)[c]		
$[W_2(O\text{-}i\text{-}Pr)_6(\mu\text{-}CO)]_2$	1272	1243	305.5	7
$[W_2(O\text{-}i\text{-}Pr)_6(py)(\mu\text{-}CO)]_2$	1305	1265	310.4	6,7
	(1298)[c]	(1271)[c]		

[a] IR spectra were recorded for Nujol mulls between CsI plates except when noted. [b] Relative to Me_4Si. [c] IR spectra recorded for a toluene solution. [d] NR = not reported. [e] Magic-angle ^{13}C NMR value.

In the presence of donor ligands such as amines or pyridine, it is possible to isolate an extensive series of compounds of formula $M_2(OR)_6L_2(\mu\text{-}CO)$ (M = Mo or W) of structural type II.[5] These compounds are closely related

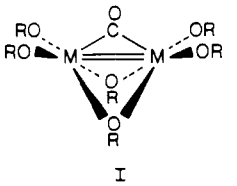

I

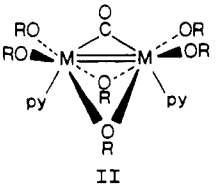

II

to I having donor ligands trans to the M–C bond of the bridging carbonyl ligand, thereby completing a confacial

(1) (a) Cotton, F. A.; Walton, R. A. *Multiple Bonds Between Metal Atoms*; Wiley: New York, 1982. (b) Chisholm, M. H., Ed. *Reactivity of Metal-Metal Bonds*, ACS Symposium Series 155; American Chemical Society: Washington, DC, 1981. (c) Chisholm, M. H., Ed. *Inorganic Chemistry Towards the 21st Century*; ACS Symposium Series 211; American Chemical Society: Washington, DC, 1983.

(2) See for example ref 1c, p 243.

(3) Ford, P. C., Ed. *Catalytic Activation of Carbon Monoxide*; ACS Symposium Series 152; American Chemical Society: Washington, DC, 1981.

(4) (a) Chisholm, M. H.; Cotton, F. A.; Extine, M. W.; Kelly, R. L. *J. Am. Chem. Soc.* **1979**, *10*, 7645. (b) Chisholm, M. H.; Huffman, J. C.; Kelly, R. L. *J. Am. Chem. Soc.* **1979**, *101*, 7615.

(5) Chisholm, M. H.; Huffman, J. C.; Leonelli, J.; Rothwell, I. P. *J. Am. Chem. Soc.* **1982**, *104*, 7030.

0276-7333/86/2305-2125$01.50/0

bioctahedral molecular geometry. The donor ligands serve the important role of suppressing the kinetically facile disproportionation reactions which occur in the presence of excess CO.

The μ-CO containing compounds I and II show anomalous spectroscopic properties with respect to the μ-CO moiety. Characteristic spectroscopic features are given in Table I and include exceedingly low values of ν(C–O) for a μ_2-CO moiety, e.g., 1655 and 1575 cm^{-1}, respectively, for Mo and W in II, as well as extremely low carbonyl carbon ^{13}C NMR chemical shifts at ca. 320 ppm downfield of Me_4Si. We suggested that these unprecedentedly low values of ν and δ together with the observed M–M, C–O, and M–C bond distances, implied a great reduction in C–O bond order and could be understood in terms of the resonance structures **a**–**c**.[5] This led us to predict[5] that the

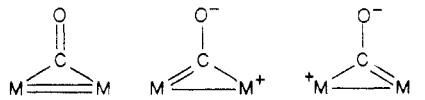

a b c

carbonyl oxygen atoms should be nucleophilic and would associate with other Lewis acids. This prediction reached fruition when Cotton and Schwotzer reported[6] the isolation and characterization of a tetranuclear compound $[W_2(O\text{-}i\text{-}Pr)_6(py)(\mu\text{-}CO)]_2$ (IIIa). Subsequently we were able to prepare and characterize the nonligated compound $[W_2(O\text{-}i\text{-}Pr)_6(\mu\text{-}CO)]_2$ (IIIb)[7] by the addition of *i*-PrOH to $W_2(O\text{-}t\text{-}Bu)_6(\mu\text{-}CO)$.

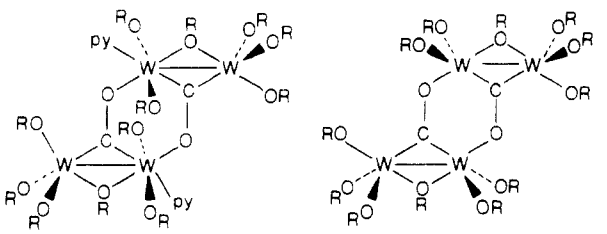

IIIa IIIb

For monocarbonyl adducts of W, the overall reaction sequence $W{\equiv}W + C{\equiv}O \rightarrow W_2(\mu\text{-}CO) \rightarrow [W_2(\mu\text{-}CO)]_2$ represents a stepwise reduction of M–M and C–O bond orders from 3 → 2 → 1 and is suggestive of a model for the reductive cleavage of CO to carbide (C^{4-}) and oxide (O^{2-}) ligands on a metal oxide, presumably a fundamental step in Fischer–Tropsch chemistry.[8]

With this background, we decided to investigate the bonding in the molecules of type I, II, and III by use of the nonparameterized Fenske–Hall molecular orbital method. In particular we were interested in the nature of the $M_2(\mu\text{-}CO)$ bonding in an attempt to elucidate the mechanism of C–O and M–M bond order reduction as well as to gain further insight and understanding into the unusual spectroscopic properties of the μ-CO moiety in these fascinating compounds.

Computational and Experimental Procedures

We have employed the model systems $M_2(OH)_6(\mu\text{-}CO)$ and $M_2(OH)_6(NH_3)_2(\mu\text{-}CO)$ where M = Mo and W to investigate the nature of $M_2(\mu\text{-}CO)$ bonding and the effects of Lewis base association in structural types I and II, as well as the tetranuclear model $[W_2(OH)_6(\mu\text{-}CO)]_2$ for type III. The coordinates for $M_2(OH)_6(\mu\text{-}CO)$ were idealized to C_{2v} point symmetry, but otherwise bond lengths and angles were taken from the crystal structures of $M_2(O\text{-}t\text{-}Bu)_6(\mu\text{-}CO)$ where M = Mo[3] and W[7]. Since the structural parameters of the central core of type I and II compounds are not significantly different, coordinates for $M_2(OH)_6(NH_3)_2(\mu\text{-}CO)$ compounds were obtained by introduction of NH_3 ligands to type I while maintaining C_{2v} geometry and with M–N distances taken from the crystal structures of $M_2(O\text{-}i\text{-}Pr)_6(py)_2(\mu\text{-}CO)$ where M = Mo and W.[5] The coordinates for the $[W_2(OH)_6(\mu\text{-}CO)]_2$ tetranuclear model were idealized to C_{2h} point symmetry but otherwise used the bond lengths and angles from the crystal structure of $[W_2(O\text{-}i\text{-}Pr)_6(\mu\text{-}CO)]_2$.[7] A summary of the structural parameters employed in this study are listed in Table II.

Table II. Structural Parameters for $M_2(\mu\text{-}CO)$ Containing Compounds[a]

	$Mo_2(OH)_6(\mu\text{-}CO)L_2$	$W_2(OH)_6(\mu\text{-}CO)L_2$	$[W_2(OH)_6(\mu\text{-}CO)]_2$
	Distances[b]		
M–M	2.498	2.526	2.657
M–C	2.022	1.997	1.945
C–O	1.210	1.250	1.350
M–μ-O	2.083	2.090	2.080
M–O_t	1.882	1.870	1.901
M–N	2.290	2.290	
O–H	0.960	0.960	0.960
N–H	1.010	1.010	
	Angles[c]		
M–C–O	141.8	140.8	136.4
M–O_t–H	152.9	148.3	140.8
M–μ-O–H	138.3	138.2	132.2
O_t–M–O_t	96.6	96.6	132.0
H–N–H	107.0	107.0	

[a] L = NH_3. [b] In angstroms. [c] In degrees.

Molecular orbital calculations were performed by using the Fenske–Hall method (program MEDIEVAL) which has been discussed in detail elsewhere.[9] The Fenske–Hall method is an approximate Hartree–Fock–Roothaan SCF–LCAO procedure, and the final results depend only upon the chosen atomic basis set and internuclear distances. SCF calculations were performed in the atomic basis on the CO and $M_2(OH)_6$ fragments and on the $M_2(OH)_6(\mu\text{-}CO)$ complexes. To aid in the interpretation of the atomic orbital interactions, the converged wave functions were transformed into appropriate fragment MO bases. These functions were then used in the program MOPLOT[10] to generate electron density maps for the important MO's of the $M_2(\mu\text{-}CO)$ compounds and their component fragments in various regions of space. Contour plots were then generated by using the program CONPLOT.[11] In the plots, solid lines represent positive density contours and dashed lines represent negative contours. All the calculations described in this paper were obtained at the Indiana University Computational Chemistry Center using a VAX 11/780 computer system, and the plots were done on a TALARIS 800 laser printer.

All atomic wave functions were generated by a best fit to Herman-Skillman atomic calculations using the method of Bursten, Jensen, and Fenske.[12] Contracted double-ζ representations were used for Mo 4d and W 5d AO's as well as C, O, and N 2p AO's. Basis functions for the metal atoms were derived for a 1+ oxidation state with the valence s and p exponents fixed at 1.8 for each of Mo 5s and 5p and W 6s and 6p orbitals.[13] An exponent of 1.16 was used for the H 1s atomic orbital.[14] It should

(6) Cotton, F. A.; Schwotzer, W. *J. Am. Chem. Soc.* **1983**, *105*, 4955.
(7) Chisholm, M. H.; Hoffman, D. M.; Huffman, J. C. *Organometallics* **1985**, *4*, 986.
(8) Masters, C. *Adv. Organomet. Chem.* **1979**, *17*, 61.
(9) Hall, M. B.; Fenske, R. F. *Inorg. Chem.* **1972**, *11*, 768.
(10) Lichtenberger, D. L. Ph.D. Dissertation, University of Wisconsin, Madison, WI, 1974.
(11) CONPLOT is a general contour plotting program written by Professor B. E. Bursten (The Ohio State University) for plotting a numerical grid of wave function values for a particular energy level, usually used with the COOK5/TAMUI version of the Xα-SW program. We have made slight modifications for use with MOPLOT and a Talaris 800 laser printer.
(12) Bursten, B. E.; Jensen, J. R.; Fenske, R. F. *J. Chem. Phys.* **1978**, *68*, 3320.
(13) Valence s and p orbital exponents of 1.8 were those that kept the populations of the W atomic 6s and 6p orbitals less than 0.1. These exponents were then used to fit Mo functions under the premise that Mo and W are approximately the same size. Four separate W bases were examined and did not effect the general conclusions presented here.
(14) Hehre, W. J.; Steward, R. F.; Pople, J. A. *J. Chem. Phys.* **1969**, *51*, 2657.

Table III. Overlap Populations for an Uncoordinated CO Ligand at the Internuclear Distances Relevant for Free CO and the CO Moiety in the $M_2(\mu\text{-CO})$ Containing Compounds

compd	R, Å	overlap pop.[a] 3σ	4σ	1π	5σ	2π
CO	1.130	0.370	0.120	0.237	−0.175	−0.508
$Mo_2(OH)_6(\mu\text{-CO})$	1.210	0.344	0.120	0.216	−0.150	−0.429
$W_2(OH)_6(\mu\text{-CO})$	1.250	0.330	0.121	0.206	−0.139	−0.395
$[W_2(OH)_6(\mu\text{-CO})]_2$	1.354	0.293	0.120	0.182	−0.111	−0.322

[a] Overlap population between C and O for a single electron occupying the molecular orbital.

be pointed out that in an earlier paper from our laboratory we argued that relativistic effects were important toward understanding W systems employing the Xα-SW computational method.[15] In the present study we were interested in the analysis of relative trends between Mo and W over a series of related compounds. For such analyses, the Fenske–Hall technique is extremely well-suited.[16]

Standard experimental techniques for the manipulation of the air- and water-sensitive materials were employed. The known compounds were prepared as previously described.[3-5,7] Electronic absorption spectra were obtained with a Hitachi 330 spectrophotometer. Samples were run vs. a solvent blank using matched 1-cm or 1-mm quartz cells. The cyclic voltammograms were obtained with use of a PAR 173 potentiostat, a PAR 175 programmer, and a Houston 2000 X-Y recorder. Cyclic voltammetric studies employed a three-electrode, two-compartment cell and a platinum disk working electrode of nominal area 0.2 mm^2, probed by a luggin capillary. A pseudoreference electrode was employed consisting of a silver wire immersed in the supporting electrolyte solution inside the capillary, and a platinum gauze served as auxiliary electrode. No internal resistance compensation was used. Low-temperature studies were carried out by immersing the sample compartment in a low-temperature bath while maintaining the pseudoreference electrode at room temperature. Redox potentials showed significant variation with temperature, and all potentials quoted are at room temperature. A 0.2 M solution of tetra-*n*-butylammonium tetrafluoroborate ($[(n\text{-Bu})_4N][BF_4]$) was employed as a supporting electrolyte, and scan rates were 200 mV/s.

$W_4(OCH_2\text{-}t\text{-Bu})_{12}(\mu\text{-CO})_2$. $W_2(O\text{-}t\text{-Bu})_6(\mu\text{-CO})$ (1.0 g, 1.2×10^{-3} mol) was suspended in hexane (5 mL) at 0 °C. A solution of neopentanol (0.8 M in hexane, 15 mL) was added via syringe. The solution was stirred for 2 h, and the red microcrystalline precipitate collected by filtration. A further crop of crystalline material was obtained on standing for 2 weeks at room temperature.

Infrared spectrum (Nujol mull, CsI plates): ν(CO) 1280 s, other bands 1477 s, 1389 s, 1360 s, 1290 s, 1259 m, 1217 w, 1170 m, 1075 vs, 1025 s, 1010 m, 978 w, 933 w, 904 m, 799 w, 752 w, 720 w, 665 s, 640 s, 610 m cm^{-1}.

^1H NMR (22 °C, toluene-d_8): two isomers are seen in solution and these will be discussed in detail elsewhere. The methylene region of the neopentoxide ligand is the most informative in this regard. Isomer A: δ(OCH_2-*t*-Bu) 5.019 singlet, 3.906 and 3.660 doublets ($^1J_{HH}$ = 10.1 Hz) of an AB quartet, and 2.992 singlet, with relative intensities 1:2:3, respectively. Isomer B: δ(OCH_2-*t*-Bu) 5.436 singlet, 3.865 and 3.786 doublets ($^1J_{HH}$ = 10.1 Hz) of an AB quartet, and 2.980 singlet, with relative intensities 1:2:3, respectively. The methyl region of the neopentoxide ligands have several overlapping resonances. δ($OCH_2C(CH_3)_3$) 1.433 singlet, 1.319 singlet, 0.945 singlet, and 0.795 singlet, with relative intensities 1:1:4:6, respectively.

Results and Discussion

The Free Carbonyl Ligand. After each calculation is completed in an atomic basis set, it is convenient to transform the results into a basis set consisting of the molecular orbitals of the isolated carbonyl ligand and dimetal fragment. This fragment and free ligand representation facilitates a direct comparison of the carbonyl ligand before and after coordination to the dimetal centers and has been applied successfully in the correlation of bonding trends in other transition-metal compounds.[17] The advantage of this procedure is that it effectively isolates in a few of the carbonyl and dimetal fragment orbitals those population changes which result from bonding interactions with the dimetal center. In this way only those carbonyl orbitals which are energetically accessible and overlap significantly with the metal orbitals are appreciably affected. The molecular orbitals for the free carbonyl ligand were calculated by using the same C–O distances as found in each metal complex. Table III lists the overlap populations of the free CO ligand at the internuclear distances used in this study and reveals that both the 5σ and 2π MO's of carbon monoxide are antibonding at these distances.

M–OH π-Bonding and the C_{2v}-$M_2(OH)_6$ Fragment. Perhaps the easiest way to visualize the bonding interactions between the CO ligand and the M_2 unit in the $M_2(\mu\text{-CO})$ containing compounds is to examine the interactions in terms of fragment MO's. We will employ the model compounds $M_2(OH)_6(\mu\text{-CO})$ where M = Mo and W as models for structural type I species. This model can be decomposed into $M_2(OH)_6$, having C_{2v} symmetry, and CO fragments. The important metal-based fragments are shown schematically in IV along with a local coordinate

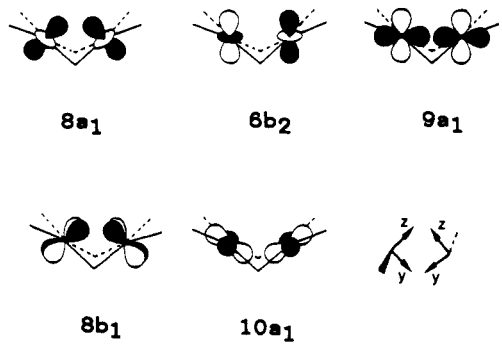

IV

system on each metal atom. With use of this local coordinate system, the important metal-localized fragment MO's of C_{2v}-$M_2(OH)_6$ can be easily visualized in terms of combining two square-planar metal fragments "hinged" along a common edge. In- and out-of-phase combinations of two metal d_{z^2} atomic orbitals yield the $8a_1$ and $6b_2$ M–M σ-bonding and antibonding fragment MO's, respectively. In a similar fashion, the in-phase combinations of two d_{yz}

(15) Braydich, M. D., Bursten, B. E.; Chisholm, M. H.; Clark, D. L. *J. Am. Chem. Soc.* **1985**, *107*, 4459.

(16) (a) Yarborough, L. W., II; Hall, M. B. *Inorg. Chem.* **1978**, *17*, 2269. (b) Sherwood, D. E., Jr.; Hall, M. B. *Inorg. Chem.* **1980**, *19*, 1805. (c) Bursten, B. E.; Cotton, F. A.; Hall, M. B.; Najjar, R. C. *Inorg. Chem.* **1982**, *21*, 302. (d) Bursten, B. E.; Gatter, M. G. *Organometallics* **1984**, *3*, 895. (e) Harris, S.; Bradley, J. S. *Organometallics* **1984**, *3*, 1086. (f) Bursten, B. E.; Gatter, M. G. *J. Am. Chem. Soc.* **1984**, *106*, 2554.

(17) (a) DeKock, R. L.; Sarapu, A. C.; Fenske, R. F. *Inorg. Chem.* **1971**, *10*, 38. (b) Fenske, R. F.; DeKock, R. L. *Inorg. Chem.* **1972**, *11*, 437. (c) Sarapu, A. C.; Fenske, R. F. *Inorg. Chem.* **1972**, *11*, 3021. (d) Peterson, J. L.; Lichtenberger, D. L., Fenske, R. F.; Dahl, L. F. *J. Am. Chem. Soc.* **1975**, *97*, 6433.

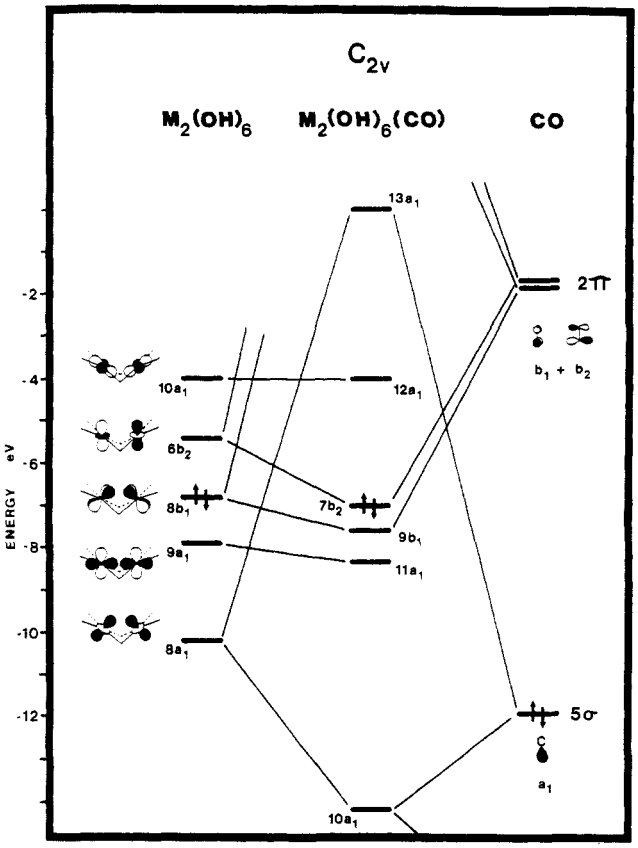

Figure 1. Fragment molecular orbital diagram showing the perturbation of C_{2v}-$M_2(OH)_6$ fragment orbitals by interaction with a CO moiety. The HOMO's in each case are marked by arrows. Only the important metal- and carbonyl-localized fragments are shown, and the actual energies are for the case where M = W.

and d_{xz} atomic orbitals would give rise to the $9a_1$ and $8b_1$ fragment MO's which are M–M σ- and π-bonding, respectively. The last fragment orbital of importance to our discussion can be thought of as an in-phase combination of two $d_{x^2-y^2}$ atomic orbitals and yields and $10a_1$ fragment MO of C_{2v}-$M_2(OH)_6$. With six electrons for metal–metal bonding, we find that they occupy the $8a_1$, $9a_1$, and $8b_1$ metal–metal bonding fragment orbitals as seen on the left of Figure 1. The unoccupied fragment orbitals are then the $6b_2$ and $10a_1$ metal–metal antibonding and bonding orbitals, respectively. One might inquire as to why the bonding $10a_1$ fragment is higher in energy than the antibonding $6b_2$ fragment. The answer lies in the degree of π bonding from the set of four terminal hydroxide ligands. From our calculations we find that the set of four terminal hydroxide ligands are involved in strong π-bonding interactions with the dimetal fragments. These interactions are most easily visualized in terms of the spatially and energetically inequivalent lone-pair orbitals on the hydroxide ligands.

The nonequivalence of lone-pair orbitals in organic molecules is well-established by both spectroscopic and theoretical investigations.[18] When the hydroxide is bound to a transition metal, we obtain a set of lone-pair orbitals similar to those of H_2O. In the M–O–H moiety there is a relatively deep σ lone-pair orbital and a higher lying π lone-pair orbital. These two lone-pair orbitals are both spatially and energetically inequivalent. Thus in discussing the π-bonding to the metal, it is essential that we distinguish between σ and π lone pairs. We have labeled these lone pairs as σ or π with respect to their local symmetry about the M–O–H plane following the nomenclature in general use for H_2O,[19] and these two types are illustrated in V. It is convenient to discuss the σ and π lone pairs

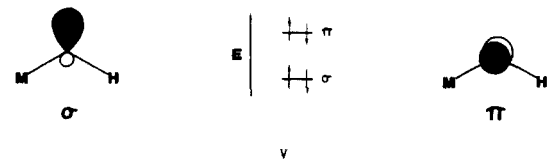

V

separately. We find in our calculations that the higher lying π lone pairs have the strongest interaction with the metal centers as expected from simple perturbation theory, and we shall discuss these interactions first. The orientation of the O–H bonds in these systems is such that they are directed "up" in a semiparallel orientation relative to the incoming μ-CO ligand as shown in VI.

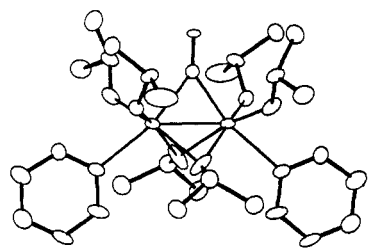

VI

As a consequence of the O–H orientation, the π lone pairs of each terminal hydroxide lie essentially in the square plane defined by each $(\mu\text{-}OH)_2M(OH)_2$ unit. This set of four π lone-pair orbitals belongs to $a_1 + b_1 + a_2 + b_2$ irreducible representations of the C_{2v} point group. These π lone pairs can form π bonds to M_2 fragment orbitals built from $d_{x^2-y^2}$ atomic orbitals since they lie in the same plane. The set of $d_{x^2-y^2}$ atomic orbitals gives rise to a_1 and b_2 irreducible representations and can form π-bonds with the appropriate a_1 and b_2 π lone-pair combinations. Thus, of the set of four π lone pairs, we find that only two are of the correct symmetry to form M–L π-bonds. The a_1 combination represents one of the strongest π-bonding interactions in the fragment resulting in a predominantly ligand-based M–L π-bonding orbital at low energy, and the predominantly metal-based counterpart is the $10a_1$ fragment which is both metal–metal σ-bonding and M–L π-antibonding. Thus, strong π-bonding from the hydroxide ligands causes the metal–metal bonding $10a_1$ fragment to be destabilized and lie above the $6b_2$ antibonding fragment. This π-bonding interaction is illustrated for the a_1 π lone-pair combination in VII.

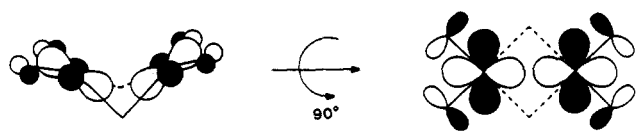

VII

The σ lone-pair orbitals are perpendicular to the π lone pairs and can interact with metal fragment orbitals constructed of either d_{xz} or d_{yz} atomic orbitals. These atomic orbitals transform as $a_1 + b_1 + a_2 + b_2$ irreducible repre-

(18) See, for example: (a) Mulliken, R. S. *Phys. Rev.* **1983**, *43*, 297. (b) Lennard-Jones, J.; Pople, J. A. *Proc. R. Soc. London, Ser. A* **1950**, *A202*, 166. **1950**, 232. (c) Walsh, A. D. *J. Chem. Soc.* **1953**, 2260. (d) Eisenstein, O.; Anh, N. T.; Jean, Y.; Devaquet, A.; Cantacuzene, J.; Salem, L. *Tetrahedron*, **1974**, *30*, 1717. (e) Brundle, C. R.; Turner, D. W. *Proc. R. Soc. London, Ser. A* **1968**, *A307*, 27. (f) Al-Joboury, M. I.; Turner, D. W. *J. Chem. Soc. B* **1967**, 373.

(19) (a) Ellison, F. O.; Schull, H. *J. Chem. Phys.* **1955**, *23*, 2348. (b) Dunning, T. H.; Pitzer, R. M.; Aung, S. *J. Chem. Phys.* **1972**, *57*, 4055.

sentations as do the σ lone pairs. From this set of four σ lone pairs, four M–L π-bonds are possible by symmetry. However, we find that only the a_1 and b_1 combinations have any appreciable interaction, and even these are considerably weaker than the π lone-pair interactions just discussed. Thus for the set of four terminal hydroxide ligands, there are two very strong and two weak π-bonding interactions. A rough measure of the magnitude of this π-bonding is given by the Mulliken populations (or orbital occupancies) of the atomic orbitals. We find that the π lone-pair occupation is 1.71 whereas the σ lone-pair occupation is 1.82. This supports the advocation that the π lone-pair orbitals are stronger donors than the σ lone pairs.

The all-important message from this discussion of π-bonding is that the metal-based fragment orbitals are destabilized by strong π-donor interactions and this will have important ramifications toward $M_2(\mu\text{-CO})$ bonding.

$M_2(OH)_6(\mu\text{-CO})$ Complexes and the Nature of M–C and M–M Bonding. As in other metal carbonyl complexes, we find that only the CO 5σ and 2π orbitals have any appreciable interaction with the $M_2(OH)_6$ fragment. Previous calculations of various degrees of sophistication have all established that CO bonds to a mononuclear transition metal via a synergistic mechanism whereby the CO ligand can form a σ-bond by electron-pair donation from its 5σ (carbon lone-pair) orbital to an empty metal d orbital, and π back-bonding results from electron donation from filled metal d orbitals to the unoccupied 2π (or π^*) orbitals of CO.[20] The carbonyl moiety interacts with the $M_2(OH)_6$ fragment in an analogous fashion. As shown in Figure 1, the CO 5σ carbon lone-pair orbital has a_1 symmetry and can interact with M_2 fragment MO's of the same symmetry. The magnitude of the interaction will depend upon the orbital energetics and the degree of overlap between the two fragments. The primary interaction is with the $8a_1$ M–M σ-bonding orbital of $M_2(OH)_6$ since it is both energetically more accessible and has the best overlap with the CO 5σ orbital. The result of this interaction is the formation of the $10a_1$ and $13a_1$ M–C σ-bonding and antibonding MO's of $M_2(OH)_6(\mu\text{-CO})$, respectively. The $10a_1$ orbital is predominantly CO 5σ in character, and the $12a_1$ orbital is predominantly metal d_{z^2} in character although it does acquire some valence metal s and p_z atomic orbital character as a result of the interaction. The $9a_1$ and $10a_1$ $M_2(OH)_6$ fragment orbitals also have the correct symmetry to interact with the CO 5σ orbital but have negligible overlap, and as a result, these fragment MO's are found to be almost entirely unperturbed by the CO ligand and result in the $11a_1$ and $12a_1$ MO's of the $M_2(OH)_6(\mu\text{-CO})$ compound. The resulting $11a_1$ orbital is the principal M–M σ-bonding orbital, and the $12a_1$ orbital "finds itself" as the LUMO of the complex. While the $11a_1$ orbital is predominantly M–M σ-bonding, we find that the $10a_1$ and $9b_1$ orbitals are involved in both M–M and M–CO bonding. The presence of bridging ligands in general makes formal bond order definition somewhat ambiguous and is traceable all the way back to diborane. Contour plots of the metal–metal σ-bonding orbital in both the $M_2(OH)_6$ fragment and the model compound $M_2(OH)_6(\mu\text{-CO})$ are shown in Figure 2. From Figure 2 it is clear that interaction with CO has little effect on the metal–metal σ-bonding interaction.

The CO 2π orbitals have b_1 and b_2 symmetry which we shall define as $2\pi_\perp$ (b_1) and $2\pi_\parallel$ (b_2) since they can interact

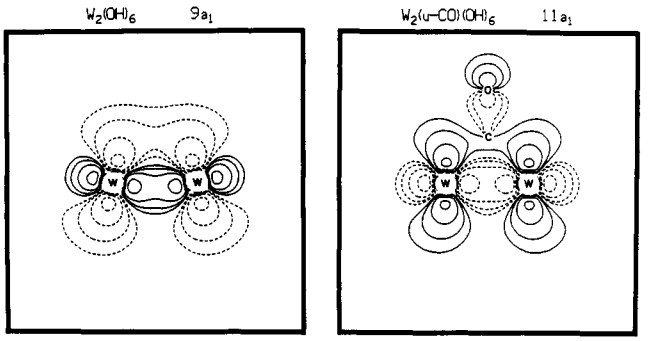

Figure 2. A comparison of contour plots of the predominantly M–M σ-bonding orbital of the C_{2v}-$M_2(OH)_6$ fragment and complete $M_2(OH)_6(\mu\text{-CO})$ compound taken as a slice through the plane containing the $M_2(\mu\text{-CO})$ moiety. The actual plots shown here are for the case where M = W as indicated above each plot. Dashed lines represent negative wave function values, and solid lines represent positive values. Contour values are ±0.02, ±0.04, ±0.08, and ±0.16 e/Å^3 in this and all subsequent plots.

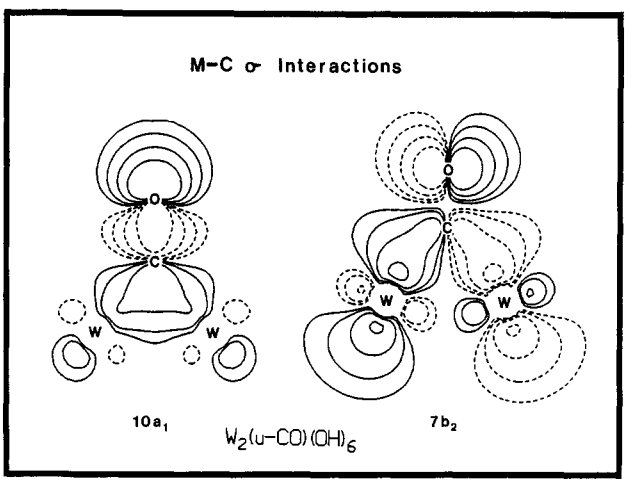

Figure 3. Contour plots of the $10a_1$ and $7b_2$ M–C σ-bonding orbitals of $M_2(OH)_6(\mu\text{-CO})$ where M = W. Plots represent a slice taken through the plane containing the $M_2(\mu\text{-CO})$ moiety.

with $M_2(OH)_6$ fragment MO's that are either perpendicular (b_1) or parallel (b_2) with respect to the M–M axis. The $2\pi_\parallel$ (b_2) MO of CO has a strong, covalent interaction with the $6b_2$ $M_2(OH)_6$ fragment MO resulting in the $7b_2$ M–C σ-bonding orbital of $M_2(OH)_6(\mu\text{-CO})$. In a similar fashion, the $2\pi_\perp$ (b_1) MO of CO interacts predominantly with the $8b_1$ $M_2(OH)_6$ fragment orbital resulting in the formation of the $9b_1$ M–C π-bonding orbital of $M_2(OH)_6(\mu\text{-CO})$. Thus for the $M_2(OH)_6(\mu\text{-CO})$ compound we have the components of two M–C σ- and one M–C π-bonding orbital, and the net M–C interaction is best described as carbyne-like in character consistent with the ^{13}C NMR chemical shifts of these compounds.[7] These three M–C bonding orbitals are shown schematically in VIII. Contour plots of the two

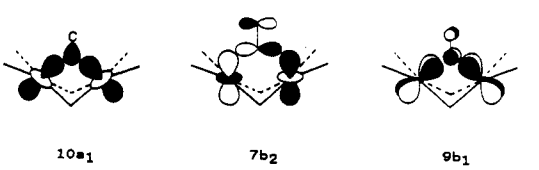

VIII

M–C σ-bonding orbitals taken as a slice through the plane containing the $M_2(\mu\text{-CO})$ moiety are shown in Figure 3. These show that the $10a_1$ orbital is predominantly CO 5σ in character and that the $7b_2$ M–C σ-bonding orbital represents a strong, covalent interaction between the CO $2\pi_\parallel$ and the $M_2(OH)_6$ fragment. This observation will have

(20) (a) Rohlfing, C. M.; Hay, P. J. *J. Chem. Phys.* **1985**, *83*, 4641. (b) Bauschlicher, C. W., Jr.; Bagus, P. S. *J. Chem. Phys.* **1984**, *81*, 5889. (c) Arratia-Perez, R.; Yang, C. Y. *J. Chem. Phys.* **1985**, *83*, 4005. (d) Yang, C. Y.; Arratia-Perez, R.; Lopez, J. P. *Chem. Phys. Lett.* **1984**, *107*, 112.

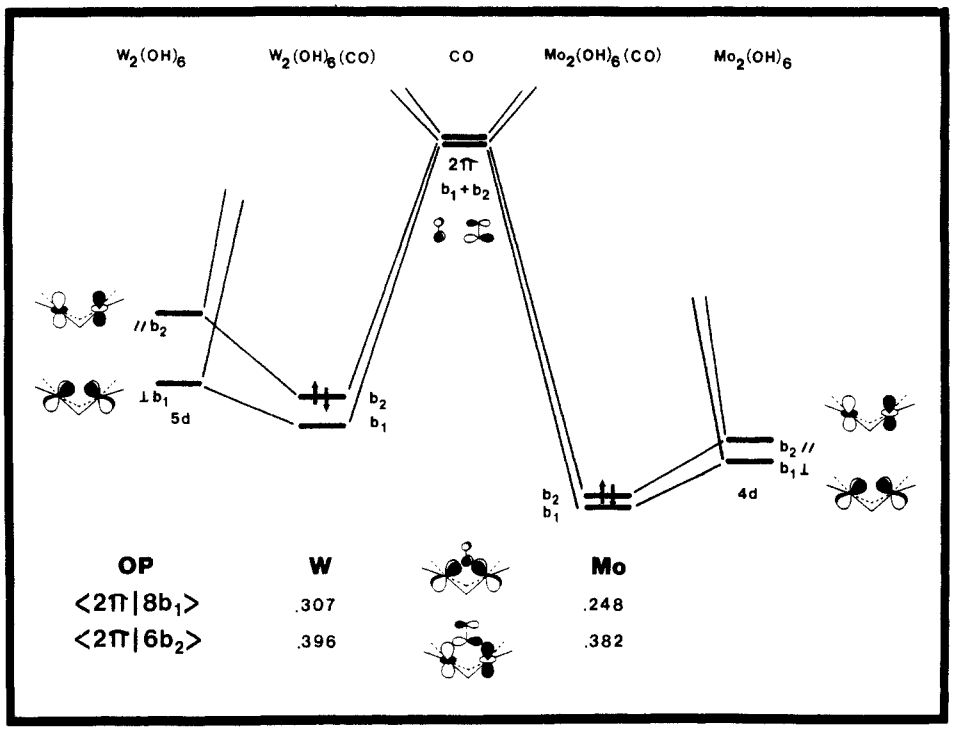

Figure 4. Comparison of carbonyl 2π orbital interactions with Mo 4d (right) and W 5d (left) $M_2(OH)_6$ fragment orbitals.

Table IV. Overlap Populations between C_{2v}-$M_2(OH)_6$ and CO Fragments

⟨CO|$M_2(OH)_6$⟩	M = Mo	M = W
⟨2π|$8b_1$⟩	0.248	0.307
⟨2π|$6b_2$⟩	0.382	0.396
⟨5σ|$8a_1$⟩	0.540	0.456

important ramifications for the discussion of CO stretching frequencies presented later.

At this point we are in a position to discuss the qualitative similarities and differences between the Mo and W homologues of formula $M_2(OH)_6(\mu\text{-CO})$. The overall bonding picture is found to be virtually identical with the only difference being their fragment orbital energies and the degree of overlap with the CO ligand. This is best illustrated via the interaction diagram shown in Figure 4 where only the CO 2π interactions with the $M_2(OH)_6$ fragment are shown. The fragment MO's constructed from W 5d atomic orbitals (left) are higher in energy than the corresponding fragments constructed of Mo 4d atomic orbitals (right). Thus for each interaction, the W-based fragments are energetically closer and have better overlap with the CO 2π orbitals than their Mo counterparts. In a similar vein, the W-based $8a_1$ fragment (not shown in Figure 4) is energetically further away from the CO 5σ orbital and results in a weaker interaction than its Mo counterpart. The message from this orbital picture is that the CO ligand is both a better 2π acceptor and a weaker 5σ donor for the W complex than for the Mo complex. These observations are demonstrated by the overlap populations between the two fragments and are listed in Table IV. From this table it can be seen that on an orbital by orbital basis, the CO 5σ orbital has better overlap with the Mo fragment than with the W fragment, and conversely, the CO 2π orbitals have better overlap with the W fragment than with the Mo fragment.

These assertions are amplified further by examination of the Mulliken populations (or orbital occupancies) of the canonical orbitals of the CO moiety in the $M_2(\mu\text{-CO})$ compounds shown in Table V. As a reference point, note that for the free CO ligand the 5σ orbital is doubly occupied and the 2π orbitals are unoccupied. For *all* of the $M_2(\mu\text{-CO})$ species however, we find that the CO 5σ population is *always* less than 2.0 and that the 2π populations are *always* greater than 0.0. Thus the Mulliken populations are revealing the synergistic nature of $M_2(\mu\text{-CO})$ bonding in these systems. In other words, 5σ donation to the dimetal center is revealed via a loss of electron density from the 5σ orbital of CO, and 2π acceptance is revealed via a gain of electron density into the 2π orbitals of CO. These populations reveal yet another measure of the *relative* magnitude of 5σ donation and 2π acceptance by the CO ligand in the Mo_2 *relative* to the W_2 species. We can see from Table V that for homologous compounds, CO is a better σ donor to Mo than W as evidenced by the decrease in CO 5σ population for the Mo_2 compounds relative to the W_2 compounds of similar formula. Likewise, we see that CO is a better 2π acceptor from W_2 centers than Mo_2 centers. Again, these results can be attributed to the *relative* energetics and magnitude of overlap between W 5d vs. Mo 4d fragment orbitals with CO. Both the smaller CO 5σ donation and 2π acceptance in ditungsten systems represent C–O bond weakening and M–C bond strengthening interactions for W compounds *relative* to Mo com-

Table V. Mulliken Populations of the Canonical Orbitals of Free CO and the CO Moiety in CO, $M_2(OH)_6(\mu\text{-CO})$, $M_2(OH)_6L_2(\mu\text{-CO})$, and $[W_2(OH)_6(\mu\text{-CO})]_2$ Compounds Where L = NH_3

compd	3σ	4σ	$1\pi_\perp$	$1\pi_\parallel$	5σ	$2\pi_\perp$	$2\pi_\parallel$	6σ
CO	2.000	2.000	2.000	2.000	2.000	0.000	0.000	0.000
$Mo_2(OH)_6(\mu\text{-CO})$	2.038	1.938	2.017	1.975	1.266	0.428	0.732	0.009
$Mo_2(OH)_6L_2(\mu\text{-CO})$	2.038	1.936	2.017	1.972	1.334	0.394	0.846	0.009
$W_2(OH)_6(\mu\text{-CO})$	2.055	1.950	2.019	1.971	1.343	0.530	0.835	0.007
$W_2(OH)_6L_2(\mu\text{-CO})$	2.057	1.955	2.019	1.967	1.412	0.492	0.975	0.007
$[W_2(OH)_6(\mu\text{-CO})]_2$	2.053	1.734	1.907	1.841	1.381	0.914	1.174	0.014

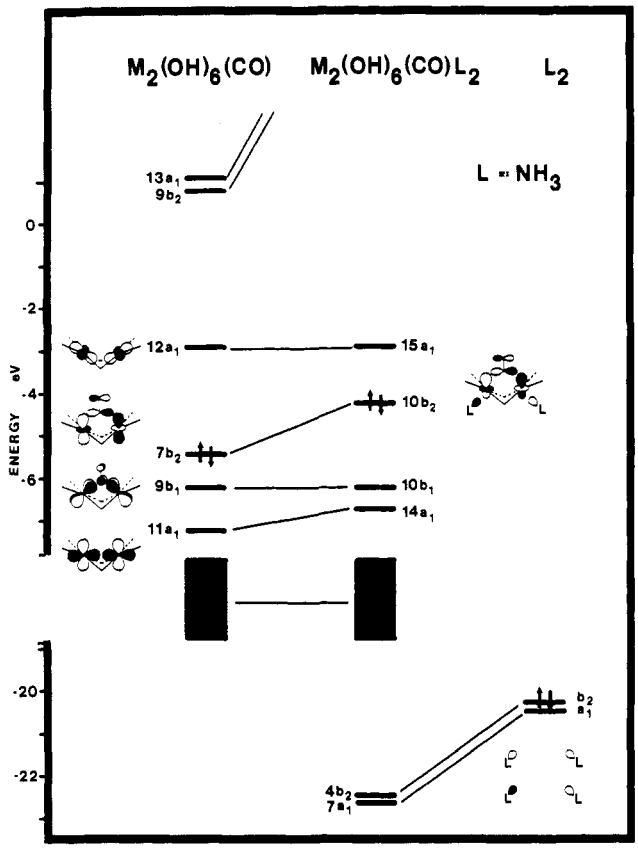

Figure 5. Fragment molecular orbital diagram showing the perturbation of the $M_2(OH)_6(\mu\text{-CO})$ orbitals by interaction with amine Lewis bases. The HOMO's are marked by arrows and the energy levels are for M = W.

pounds and are consistent with the ca. 70 cm^{-1} decrease in ν(C–O) for $W_2(\mu\text{-CO})$ relative to $Mo_2(\mu\text{-CO})$ containing homologues.[7] In general we find that π back-bonding is the dominant M–C bonding mechanism. In this respect we note that Bauschlicher and Bagus[20b] recently analyzed the bonding in $Ni(CO)_4$ and concluded that π back-bonding dominated the Ni–CO interaction. Even more recently, Rohlfing and Hay[20a] have argued that the π back-bonding portion of the M–C interaction is actually underestimated at the SCF level.

The Effect of Lewis Base Association on $M_2(OR)_6(\mu\text{-CO})$ Compounds. It is known experimentally that Lewis base association to the $M_2(\mu\text{-CO})$ moiety inhibits CO dissociation and lowers the CO stretching frequency by ca. 10 cm^{-1}.[5] The easiest way to understand the effect of Lewis base association is to use the fragment approach by simply introducing two σ-donor ligands trans to the M–C bonds of the $M_2(OH)_6(\mu\text{-CO})$ compounds already discussed. We have chosen to use NH_3 as a model for a neutral N-donor since amines have been shown experimentally to have essentially the same effect as pyridine in the $M_2(\mu\text{-CO})$ compounds.[5] Symmetry-adapted in- and out-of-phase combinations of a set of σ lone-pair orbitals of $(NH_3)_2$ yield either a_1 or b_2 combinations, respectively and are denoted as L_2 orbitals in the bottom right of Figure 5. These a_1 and b_2 representations of L_2 lone-pair orbitals can interact with a_1 or b_2 fragments of $M_2(OH)_6(\mu\text{-CO})$ on the left of Figure 5. We find that the primary interaction is between the L_2 orbitals and empty $13a_1$ and $9b_2$ fragment orbitals of the M_2 center. These fragment orbitals can be best described as "dsp" hybrid orbitals of the $M_2(OH)_6(\mu\text{-CO})$ species which point directly at the empty site of the incoming donors and consequently have the best overlap. More important to our discussion of $M_2(\mu\text{-CO})$ bonding, however, is the observation that the $7b_2$ M–C σ-bonding orbital of the $M_2(OH)_6(\mu\text{-CO})$ fragment is destabilized by the b_2 interaction with L_2 donors. This b_2 interaction induces a rehybridization of the $7b_2$ M–C σ-bonding fragment. Valence metal s and p_z atomic orbital character mixes into the MO in such a way as to direct the orbital away from the L_2 fragment and more toward carbon. This rehybridization has two effects: it decreases the magnitude of antibonding between the L_2 and M_2 fragments in the orbital, and more importantly, it enhances the M–C σ overlap in the orbital. The b_2 M–C σ-bonding orbital is actually destabilized as a result of this interaction as shown in Figure 5. The rehybridization of this orbital is demonstrated with the aid of contour plots (Figure 6) taken in the plane containing the $M_2(\mu\text{-CO})L_2$ unit before and after Lewis base association. It appears, therefore, that Lewis base association forces a rehybridization in the b_2 M–C σ-bonding orbital resulting in increased M–C σ overlap which in turn inhibits CO dissociation. In other words, destabilization of the b_2 orbital increases the degree of back-bonding and hence an increase in the reducing strength of the b_2 interaction on the CO ligand.

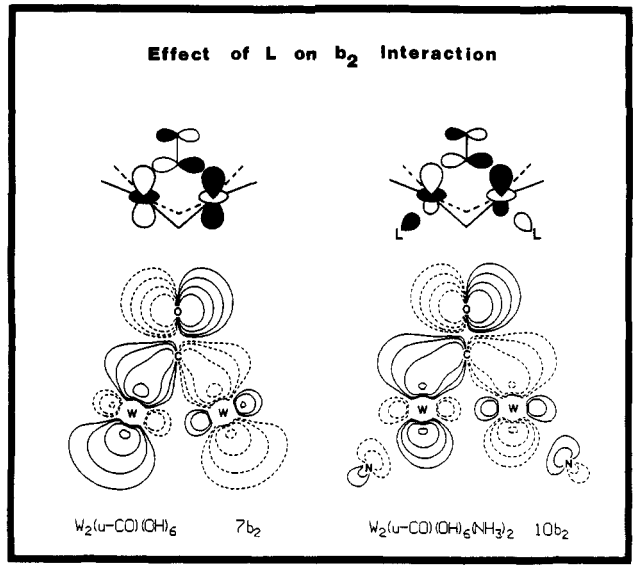

Figure 6. Contour plots and schematic illustrations representing the rehybridization of the M–C σ-bonding b_2 orbital induced by Lewis base association. Plots shown are of the $7b_2$ orbital of $W_2(\mu\text{-CO})(OH)_6$ (left) and the $10b_2$ orbital of $W_2(OH)_6(NH_3)_2(\mu\text{-CO})$ (right).

This observation is amplified by examination of the Mulliken populations of the canonical orbitals of CO in the $M_2(\mu\text{-CO})L_2$ species shown in Table V. Lewis base association increases the population of the $2\pi_{\parallel}$ (b_2) orbitals of CO for both the Mo and the W species relative to the nonligated forms. Again, this is consistent with the Lewis base enhancing the back-bonding of the b_2 interaction and thus a qualitative lowering in ν(C–O) relative to the nonligated forms.

Bonding in the $[W_2(\mu\text{-CO})]_2$ Containing Compounds. The electronic structure and bonding in the $W_4(CO)_2(OH)_{12}$ model compound having C_{2h} symmetry is most easily understood in terms of combining two $W_2(OH)_6(\mu\text{-CO})$ fragments. In going from C_{2v}-$W_2(OH)_6(\mu\text{-CO})$ to C_{2h}-$[W_2(OH)_6(\mu\text{-CO})]_2$, the geometry about the metal atom changes from square-pyramidal to trigonal-bipyramidal. The easiest approach is to compare the hypothetical C_{2v}-$M_2(OH)_6$ and $M_2(OH)_7^-$ fragments shown in IXa and IXb, respectively. Each fragment in IX has six electrons for M–M bonding, and it is readily seen that the number, symmetry properties, occupation by electrons, and

IXa IXb

approximate energies of these frontier fragment orbitals are all similar and hence isolobal.[21] The three important, occupied metal-based fragments are shown in Xa–c. The

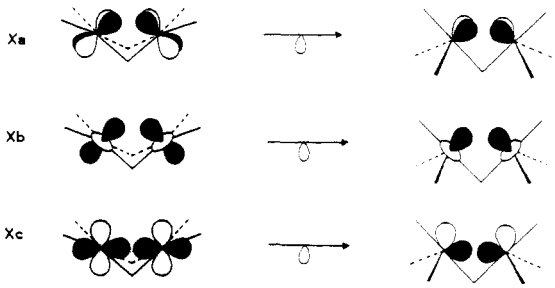

utility of this observation is that the nature of $M_2(\mu\text{-CO})$ bonding will be essentially the same in each dinuclear fragment, and thus one can imagine "dimerizing" our new $M_2(\mu\text{-CO})$ fragment (IXb) to yield the MO's of the $[M_2(\mu\text{-CO})]_2$ containing compound. For each M_2 fragment, in- and out-of-phase combinations of the M_2 fragment MO's will give rise to resultant MO's of the tetranuclear compound. For example, the a_g and b_u combinations of Xc will give rise to the two components of M–M σ-bonding MO's of the tetranuclear cluster which correspond to the two highest occupied MO's in $[W_2(OH)_6(\mu\text{-CO})]_2$. This observation, coupled with the aid of some pertinent contour plots, greatly simplifies the bonding picture of the $[W_2(OH)_6(\mu\text{-CO})]_2$ compound. As an example we note that an in-phase combination of the contour plot of the $10a_1$ M–C σ-bonding MO of C_{2v}-$M_2(OH)_6(\mu\text{-CO})$ (Figure 3) would yield the $12a_g$ MO of $[W_2(OH)_6(\mu\text{-CO})]_2$ shown in Figure 7. The CO 5σ character of this MO is still very apparent from the plot and can be compared to a plot of the CO 5σ orbital also shown in Figure 7. In a similar vein, a_g and b_u combinations of the $7b_2$ M–C σ-bonding MO of $W_2(OH)_6(\mu\text{-CO})$ (also shown in Figure 3) can be envisaged to give rise to the $20a_g$ and $20b_u$ MO's of $[W_2(OH)_6(\mu\text{-CO})]_2$ shown in Figure 8. Again, the CO 2π parentage is readily apparent from the plot. In fact, the CO parentage in these MO's gives us an alternative viewpoint with which to understand the MO's and their consequences toward CO reduction.

A schematic energy level diagram for the C_{2h}-$W_4(\mu\text{-CO})_2(OH)_{12}$ molecule is shown in Figure 9. Only those orbitals important for M–M or $M(\mu\text{-CO})$ bonding are given. On the right of the figure is a listing of the orbital type (σ or π) and the CO parentage (or carbonyl character) of each orbital. The two highest occupied orbitals are W–W σ bonding in character with essentially negligible CO contribution. Each of these M–M σ-bonding orbitals is σ-bonding between two discrete ditungsten centers, just as though we had taken in- and out-of-phase (a_g and b_u) combinations of the W–W σ-bonding orbitals of our dinuclear centers, and is best seen with the aid of the contour plots shown in Figure 10. The remaining molecular orbitals are designated as either $W_4(\mu\text{-CO})_2$ σ or π with respect to the plane containing the $W_4(\mu\text{-CO})_2$ moiety. These orbitals are highly delocalized over the entire $W_4(\mu\text{-CO})_2$ unit, and it is therefore difficult in most instances to designate one orbital as predominantly W–C or W–O σ bonding. Each of these MO's contains character of both types. However, the net result is that we obtain a set of six σ-bonding and four π-bonding orbitals with respect to the $W_4(\mu\text{-CO})_2$ moiety.

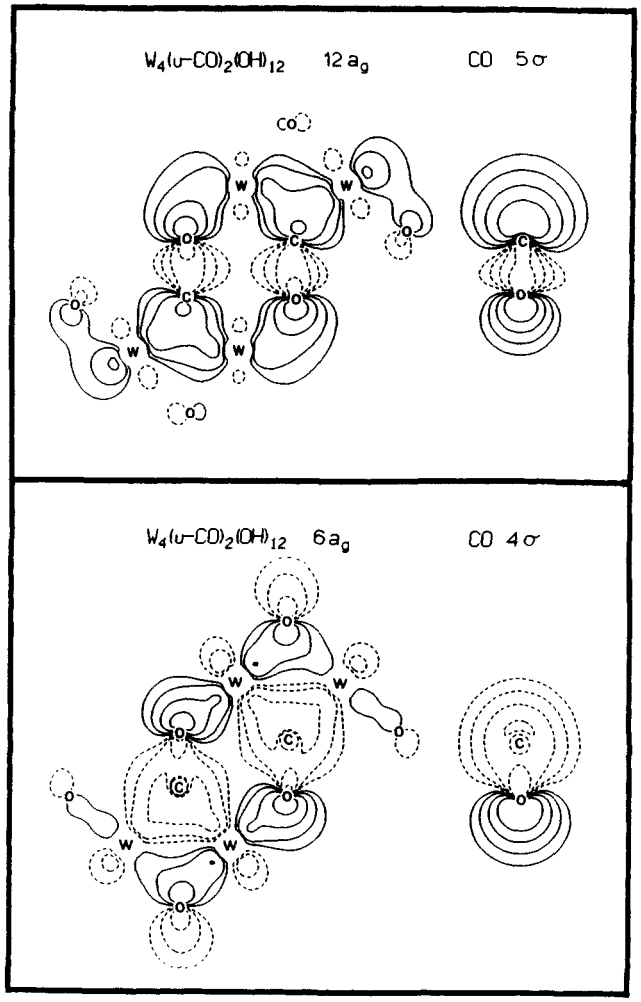

Figure 7. Contour plots of the $12a_g$ (top) and $6a_g$ (bottom) molecular orbitals of $[W_2(OH)_6(\mu\text{-CO})]_2$ taken as a slice through the plane containing the $[W_2(\mu\text{-CO})]_2$ moiety. Contour plots of the relevant orbitals of CO at the same scale and C–O distance are shown on the right of each figure.

By examination of the CO parentage we can see that the effect of dimerization of $W_2(\mu\text{-CO})$ units to give $[W_2(\mu\text{-CO})]_2$ clusters is that CO is now bound to W through both C and O. As a result, charge can now be transferred into the CO 2π orbitals from both ends. This is readily seen with the aid of the contour plots in Figure 8. Let us continue our tracing of CO parentage in the $[W_2(\mu\text{-CO})]_2$ compound for it appears to be the most informative in terms of understanding the factors responsible for CO reduction. The a_g combination of CO 5σ was already demonstrated in Figure 7. The b_u combination of CO 5σ can mix with the b_u combination of CO $1\pi_\parallel$ since now, under C_{2h} symmetry and the presence of two CO moieties, CO $1\pi_\parallel$ and 5σ can and do interact. The result of the interaction is to polarize the CO orbitals toward "inner" or "outer" W atoms (with respect to the $[W_2(\mu\text{-CO})]_2$ ring) yielding the $11b_u$ and $13b_u$ MO's of $[W_2(OH)_6(\mu\text{-CO})]_2$ shown with the aid of plots in Figure 11. Again, from the plots it is apparent that the $11b_u$ MO is predominantly CO 5σ and the $13b_u$ is predominantly CO $1\pi_\parallel$ in character. Now for the first time, CO is actually donating some charge via its π-bonding orbitals. It should be pointed out that

(21) (a) Hoffman, R. *Angew. Chem., Int. Ed. Engl.* **1982**, *21*, 711. (b) Albright, T. A.; Burdett, J. K.; Whangbo, M. H. *Orbital Interactions in Chemistry*; Wiley: New York, 1985; Chapter 21.

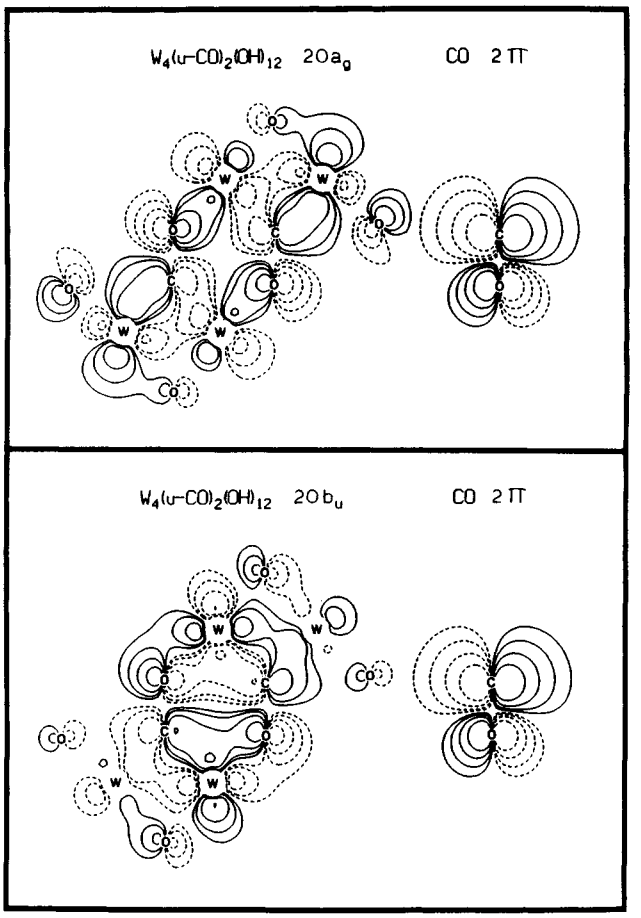

Figure 8. Contour plots of the $20a_g$ (top) and $20b_u$ (bottom) molecular orbitals of $[W_2(OH)_6(\mu\text{-CO})]_2$. Relevant CO 2π orbitals are plotted on the right at the same scale and C–O distance.

Yang and Arratia-Perez have seen evidence for 1π and 5σ mixing in $M(CO)_6$ compounds of Cr, Mo, and W employing the Dirac-scattered-wave formalism.[20c] Those authors argued that this metal–ligand bonding contribution is quantitatively as significant as the well-known σ-donation and π back-bonding mechanisms. We see no evidence of the $5\sigma/1\pi$ interaction in the dinuclear compounds, but it becomes increasingly more important for the tetranuclear compounds. This mixing of occupied 1π and 5σ orbitals represents essentially an sp to sp^2 rehybridization of C and O and is illustrated in Figure 11. We also find that the CO 4σ oxygen lone-pair orbital can be involved in W–O σ bonding. The a_g combination results in the $6a_g$ MO of $[W_2(OH)_6(\mu\text{-CO})]_2$ which is shown via a contour plot in Figure 7.

Thus far we have only discussed the σ interactions with respect to the $[W_2(\mu\text{-CO})]_2$ containing plane and our calculations indicate an extensive eight electron π system as well. Again, this is most easily rationalized by tracing the CO parentage of the orbitals through the perturbations imposed by the M_2 fragments. In- and out-of-phase combinations of *both* CO $1\pi_\perp$ and $2\pi_\perp$ yield $2a_g$ and $2b_u$ symmetry-adapted linear combinations. The CO moiety is now behaving as a π donor via the $1\pi_\perp$ orbitals and a π acceptor via the $2\pi_\perp$ orbitals, both of which represent C–O bond-weakening interactions. This π system is illustrated schematically in Figure 12, and an analogy with the π system in benzene is readily apparent with respect to the nodal properties of the orbitals. From Figure 12 it can be seen that in the $5a_u$ orbital there are no nodal planes with respect to the central $[W_2(\mu\text{-CO})]_2$ ring, whereas the $5b_g$ and $11b_g$ each contain one nodal plane, and the $11a_u$ contains two nodal planes. The analogy stops here, however,

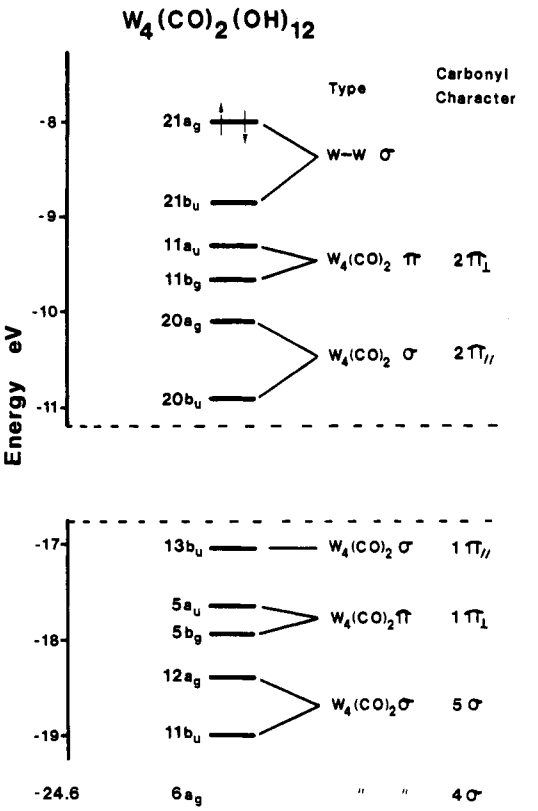

Figure 9. Energy level diagram showing the important occupied MO's of $[W_2(OH)_6(\mu\text{-CO})]_2$. The orbital type ($\sigma$ or π) refers to the nodal properties of the orbital with respect to the $[W_2(\mu\text{-CO})]_2$ containing plane. The carbonyl character is indicated at the far right. Dashed lines represent a break in the energy scale.

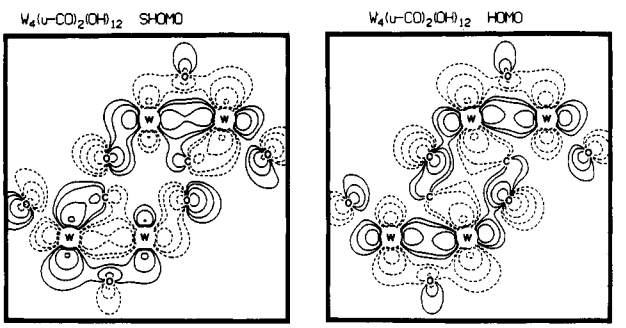

Figure 10. Contour plots showing the two components of the M–M σ bond of $[W_2(OH)_6(\mu\text{-CO})]_2$.

for the benzene π system only contains six electrons whereas the $[W_2(\mu\text{-CO})]_2$ π system contains eight.

The primary C–O bond weakening interactions in the $[W_2(\mu\text{-CO})]_2$ unit are produced by the fact that the CO moiety bonds to three W atoms by way of both carbon and oxygen atoms. This has important consequences for the π-acceptor role of the CO 2π orbitals in that charge can transfer into the 2π orbitals from two sides as opposed to most μ-CO complexes, where CO is bound to a metal through just the carbon atom. This is the principle C–O bond-weakening mechanism in the $[W_2(\mu\text{-CO})]_2$ species and represents "power" back-bonding relative to the $W_2(\mu\text{-CO})$ species. This observation is amplified by the Mulliken populations of the canonical orbitals of CO for the $[W_2(\mu\text{-CO})(OH)_6]_2$ compound listed in Table V. The dramatic effect of increased π back-bonding is evidenced by the fact that the CO $2\pi_\perp$ population has virtually doubled in $[W_2(OH)_6(\mu\text{-CO})]_2$ relative to $W_2(OH)_6(\mu\text{-CO})$. A concomitant increase in the $2\pi_\parallel$ population is also very apparent. Furthermore, it is seen that CO is now donating charge via the 4σ and 1π orbitals as illustrated by the

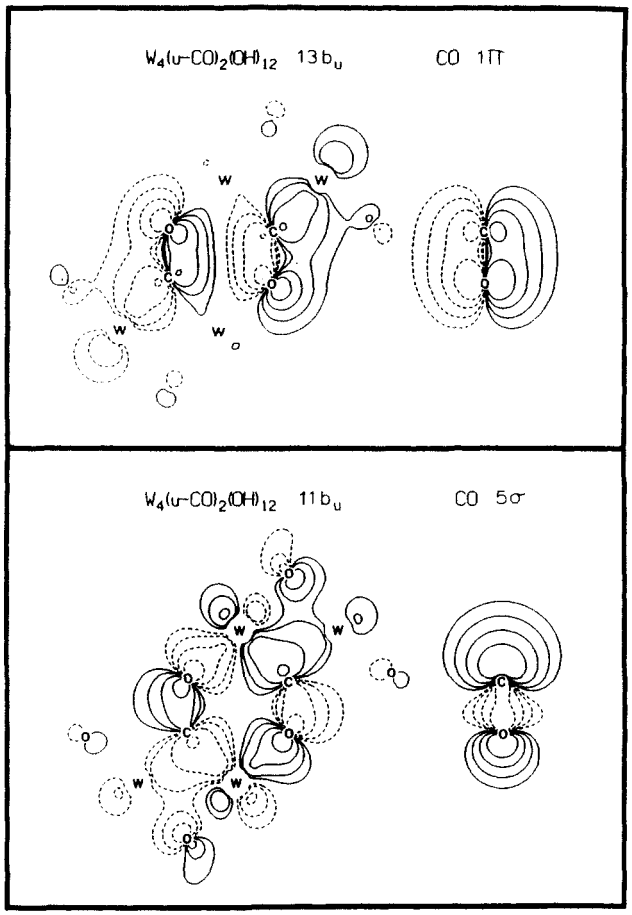

Figure 11. Contour plots of the $13b_u$ and $11b_u$ molecular orbitals of $[W_2(OH)_6(\mu\text{-CO})]_2$. The important CO orbitals are plotted on the right, and the polarization effect of the CO $5\sigma/1\pi$ mixing is readily apparent.

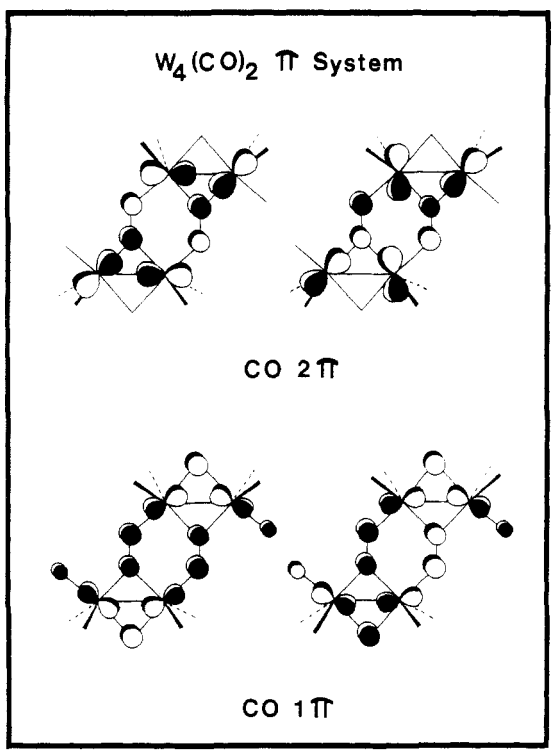

Figure 12. Schematic illustration of the $W_4(\mu\text{-CO})_2$ π system.

decrease in the 4σ and 1π populations in $[W_2(OH)_6(\mu\text{-CO})]_2$ relative to $W_2(OH)_6(\mu\text{-CO})$. The interactions represented by 4σ and 1π donation along with 2π acceptance represent

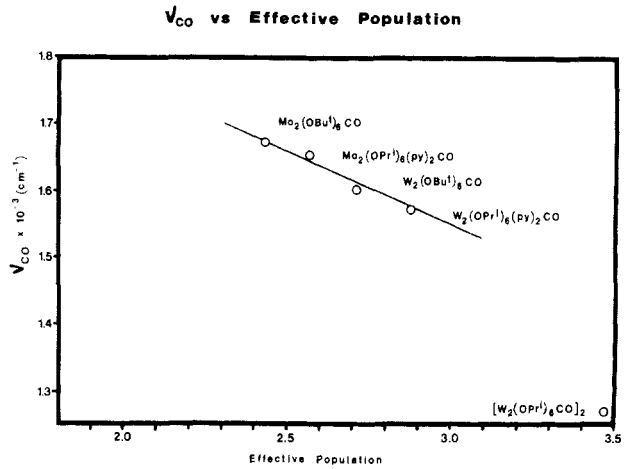

Figure 13. A plot of effective population of carbonyl antibonding orbitals vs. ν(C–O) for $M_2(\mu\text{-CO})$ containing compounds. The spectral data for $M_2(O\text{-}t\text{-Bu})_6(\mu\text{-CO})$ were used with the populations from the model $M_2(OH)_6(\mu\text{-CO})$ where M = Mo and W as indicated. Spectral data for $M_2(O\text{-}i\text{-Pr})_6(py)_2(\mu\text{-CO})$ were used with the populations from the model $M_2(OH)_6(NH_3)_2(\mu\text{-CO})$ where M = Mo and W as indicated.

C–O bond-weakening and W–C bond-strengthening mechanisms in these compounds.

Correlations between CO Orbital Occupations and ν(C–O) Values. For each series of Mo and W compounds there exists a decrease in ν(C–O) of ca. 70 cm^{-1} for W relative to Mo species as seen in Table I. We are provoked to ponder the possible relationship between our calculated electronic trends and the spectroscopic data. In other words if our calculated electronic trends reflect real effects, then we should expect some self-consistency between theory and experiment.

Several studies from the Fenske group have demonstrated that, for the terminal carbonyl ligand, trends in Cotton–Kraihanzel (CK) force constants could only be accounted for when changes in *both* 5σ and 2π orbital occupancies were considered.[22] In particular, those studies emphasized that donation of electron density from the 5σ orbital resulted in a strengthening of the C–O bond consistent with the antibonding character of the orbital. Those authors derived an empirical equation to correlate the orbital occupancies of antibonding orbitals of CO with CK force constants. Examination of the Mulliken populations of the CO orbitals in our $M_2(\mu\text{-CO})$ compounds listed in Table V demonstrates that for dinuclear $M_2(OH)_6(\mu\text{-CO})$ and $M_2(OH)_6L_2(\mu\text{-CO})$ compounds, only the 5σ and 2π populations change while the others remain essentially constant. Thus, if we define an "effective population" as the simple sum of antibonding 5σ and 2π populations, then we might expect a correlation between ν(C–O) and our "effective population". A simple plot of ν(CO) vs. "effective population" demonstrates that a linear correlation does in fact exist as shown in Figure 13. We also find that the tetranuclear compound $[W_2(OH)_6(\mu\text{-CO})]_2$ does not fall on this line and indeed it should not. The implicit assumption that only 5σ and 2π occupations will change does not hold true for the tetranuclear compound as previously discussed. The general trend seen here is quite satisfying in that as our "effective population" of antibonding orbitals increases, there is an increase in M–C bond strength, a decrease in C–O bond strength, and

(22) (a) Hall, M. B.; Fenske, R. F. *Inorg. Chem.* **1972**, *11*, 1619. (b) Saparu, A. C.; Fenske, R. F. *Inorg. Chem.* **1975**, *14*, 247. (c) Lichtenberger, D. L.; Fenske, R. F. *J. Am. Chem. Soc.* **1976**, *98*, 50. (d) Fenske, R. F. *Pure Appl. Chem.* **1971**, *27*, 61.

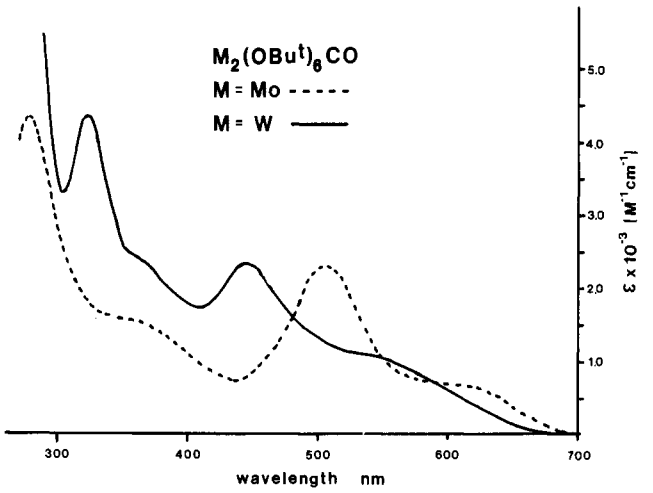

Figure 14. Room-temperature electronic absorption spectra of $M_2(O\text{-}t\text{-}Bu)_6(\mu\text{-}CO)$ compounds for M = Mo and W.

a concomitant decrease in ν(C–O).

Electronic Absorption Spectra of $M_2(OR)_6(\mu\text{-}CO)$ Compounds. Compounds of formula $M_2(O\text{-}t\text{-}Bu)_6(\mu\text{-}CO)$ (M = Mo and W) are ideal for the comparison of electronic spectra of Mo- and W-containing type I compounds. The molybdenum compound is relatively unstable in solution at room temperature with respect to facile CO dissociation, and thus, extinction coefficients for this compound are rendered unreliable.[23] However, a wealth of information can be obtained from the experimental transition energies. The W analogue $W_2(O\text{-}t\text{-}Bu)_6(\mu\text{-}CO)$ is very stable in solution over the time period of the experiment and accurate extinction coefficients have been measured. The electronic absorption spectra for $M_2(O\text{-t-Bu})_6(\mu\text{-}CO)$ compounds dissolved in hexane are shown in Figure 14 (M = Mo, dashed line; M = W, solid line). As can be seen, the relatively simple spectra are qualitatively very similar for both Mo- and W-containing compounds. Each spectrum consists of two well-defined maxima, each with a shoulder on the low-energy side. We will limit our discussion to the first two maxima seen at 440 nm (22 700 cm^{-1}) and 540 nm (18 500 cm^{-1}) for $W_2(O\text{-}t\text{-}Bu)_6(\mu\text{-}CO)$. For the Mo-containing analogue, these two absorption features *both* appear to red shift by ca. 2900 and 2400 cm^{-1}, respectively. The brilliant purple and blood-red colors of the Mo and W compounds (respectively) are understandable in terms of their absorption spectra.

To determine probable assignments for the two lowest energy absorption bands, we recall that there are three occupied, energetically isolated orbitals near the HOMO of type I compounds. The highest two are M–C σ- and π-bonding orbitals resulting from CO π back-bonding interactions. Both IR spectral data and our calculations indicate that the magnitude of this π back-bonding interaction is stronger for the W-containing compounds than the Mo-containing analogues. Due to the low symmetry of these compounds (C_{2v} at best) virtually all transitions are allowed by symmetry. Thus qualitatively, one might expect the lowest energy transitions between orbitals in the frontier region to occur at higher energy for W-containing compounds relative to the Mo analogues as a result of the stronger π back-bonding interactions for W compounds. This is precisely the trend observed in the spectra shown in Figure 14. In this regard we note that Dirac-scattered-wave calculations on $W(CO)_6$ show that relativistic effects actually stabilize metal–ligand interactions but do not appear to add to the qualitative understanding of the valence electronic structure.[19d] On this basis we propose the possible assignments of $7b_2 \rightarrow 12a_1$ ($A_1 \rightarrow B_2$) and $9b_1 \rightarrow 12a_1$ ($A_1 \rightarrow B_1$) for the two lowest energy transitions, respectively. We note that the intensity of these transitions is relatively low, with extinction coefficients on the order of ca. 1000–2000 M^{-1} cm^{-1}. In general, transitions between orbitals that differ from one another simply by behavior with respect to a symmetry plane are strongly allowed (e.g., atomic transitions s → p, p → d, etc.). The proposed transitions are between molecular orbitals that are built up of different types of metal d orbitals: $7b_2$ (d_{z^2}) → $12a_1$ ($d_{x^2-y^2}$) and $9b_1$ (d_{xz}) → $12a_1$ ($d_{x^2-y^2}$). For this reason the two orbitals will differ from one another by more than just behavior with respect to a single symmetry plane and thus are expected to be relatively weak. We do not feel that simple orbital energy differences from our calculations are a reliable estimate of the energetic differences between states. In particular, our own past experience in dealing with W-containing compounds has demonstrated that relativistic effects can amount to as much as an electron-volt,[14] and thus we feel that the qualitative arguments presented here will suffice for our proposals.

Lewis base association has very little effect on the electronic absorption spectra, and the band positions and extinction coefficients for ligated and nonligated W-containing compounds are compared in Table VI. Qualitatively, the calculations suggest that Lewis base association has little overall effect on the ordering of molecular orbitals, and the overall appearance and band intensities for the Lewis base adducts are consistent with this observation.

The band positions and relative intensities of the electronic absorption spectrum of $[W_2(O\text{-i-Pr})_6(\mu\text{-}CO)]_2$ are listed at the bottom of Table VI. Our calculations on the model compound $[W_2(OH)_6(\mu\text{-}CO)]_2$ indicate an energetically isolated LUMO, the $12b_g$ orbital illustrated in XI. Our calculations give a 3.0 eV HOMO-LUMO gap followed by another 1.4-eV separation to the next cluster of virtual

Table VI. Electronic Absorption Spectra of $M_2(\mu\text{-}CO)$ Containing Compounds of Mo and W[a]

compd	λ_{max}, nm	λ_{max}, cm^{-1}	ϵ, M^{-1} cm^{-1}
$Mo_2(O\text{-}t\text{-}Bu)_6(\mu\text{-}CO)$	620	16 100	
	505	19 800	
	360	27 800	
	280	35 700	
	240	41 700	
$W_2(O\text{-}t\text{-}Bu)_6(\mu\text{-}CO)$	540	18 500	1100
	440	22 700	2400
	360	27 800	2600
	318	31 400	4500
	280	35 700	13000
$W_2(OCH_2\text{-}t\text{-}Bu)_6(py)_2(\mu\text{-}CO)$	520	19 200	1300
	440	23 800	2200
	360	27 800	3200
	290	34 500	9000
$[W_2(O\text{-}i\text{-}Pr)_6(\mu\text{-}CO)]_2$	520	19 200	3700
	370	27 000	7400
	330	30 300	11000
	290	34 500	18000

[a] Recorded in hexane.

(23) A freshly prepared sample of $Mo_2(O\text{-}t\text{-}Bu)_6(\mu\text{-}CO)$ slowly decomposes in dilute hydrocarbon solution by loss of CO to form $Mo_2(O\text{-}t\text{-}Bu)_6$ as the sole product as monitored by UV–visible spectroscopy over a 10-h period. Reproduction on three separate occasions indicates that $Mo_2(O\text{-}t\text{-}Bu)_6(\mu\text{-}CO)$ has a half-life of ca. 1 h at the concentrations employed in this study. These observations were used to identify the spectrum of $Mo_2(O\text{-}t\text{-}Bu)_6(\mu\text{-}CO)$ and demonstrated that the spectrum recorded within a few minutes of sample preparation (as seen in Figure 14) is the authentic spectrum of $Mo_2(O\text{-}t\text{-}Bu)_6(\mu\text{-}CO)$ although extinction coefficients are rendered unreliable.

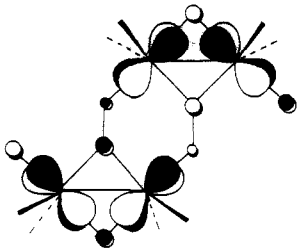

XI

orbitals. Under C_{2h} symmetry, allowed transitions are to A_u and B_u excited states. Since the LUMO is effectively isolated, we might expect the lowest energy transition to be from one of the occupied orbitals to the LUMO. In this case, symmetry considerations will be of great help. If we consider only the four highest, occupied MO's of Figure 9, then we see that only the $21b_u \rightarrow 21b_g$ and $11a_u \rightarrow 12b_g$ transitions are dipole-allowed. It is very possible that the calculation has overestimated the separation between the two W–W σ-bonding MO's, and thus we propose that the lowest energy transition at ca. 19 000 cm^{-1} (3700 M^{-1} cm^{-1}) arises from the $21b_u \rightarrow 12b_g$ (W–W $\sigma \rightarrow$ W–W π) excitation.

All of the W-containing compounds listed in Table VI exhibit relatively intense transitions (10 000–18 000 M^{-1} cm^{-1}) in the UV region near ca. 35 000 cm^{-1}. This region of the spectrum is certainly much more speculative; however, the intensities and energies of these bands are consistent with ligand-to-metal charge transfer from alkoxide ($p\pi$) orbitals. In this regard a photoelectron spectrum would be useful in delineating the position of the oxygen lone pairs relative to the metal–metal bonds.

Electrochemistry of $M_2(\mu$-CO) Containing Compounds. Dinuclear Compounds. The electrochemical properties of the dinuclear $M_2(\mu$-CO) containing compounds were examined in THF solutions, and the resulting electrochemical data are summarized in Table VII. In general, the Mo complexes are always easier to reduce and harder to oxidize than their W analogues. In addition, the reduced Mo complexes appear kinetically more stable than their W counterparts. These observations are consistent with the expected group trend, and our calculated results that the W valence orbitals are higher in energy than those of Mo, as well as the trends in ν(C–O) previously discussed. The compounds of formula $M_2(O\text{-}t\text{-}Bu)_6(\mu$-CO) exhibit quasi-reversible reduction behavior at room temperature and reversible behavior at 0 °C. These *tert*-butoxide (O-*t*-Bu) compounds provide the only pair of homologous compounds with reversible couples for accurate comparison of reduction potentials between Mo and W compounds. It can be seen from Table VII that the Mo compound is easier to reduce by ca. 0.79 V. The peak separation for this wave is 120 mV (for both Mo and W), indicating some irreversibility to the reduction process. With our experimental setup, reversible couples (such as ferrocene/ferrocenium) exhibited peak separations of 90–120 mV (vs. the 60 mV anticipated, indicating that part of the large separation is due to uncompensated internal resistance. Some complexes showed new reversible waves on subsequent cycles following irreversible reduction; e.g., room temperature reduction of $Mo_2(O\text{-}t\text{-}Bu)_6(\mu$-CO) gave rise to a new reversible wave at −0.80 V; reduction of $W_2(OCH_2\text{-}t\text{-}Bu)_6(py)_2(\mu$-CO) gave rise to a new reversible wave at −0.89 V. The identities of the complexes giving rise to these new waves are as yet unknown.

Where isopropoxide (O-*i*-Pr) compounds can be directly compared with their neopentoxide (OCH_2-*t*-Bu) analogues, in general the O-*i*-Pr complex is easier to oxidize and harder to reduce than the OCH_2-*t*-Bu analogue. The one exception is $Mo_2(O\text{-}i\text{-}Pr)_6(py)_2(\mu$-CO); however, here a reversible potential is being compared to an irreversible one, which may invalidate this observation. Thus, the general trend parallels that expected on the basis of the relative inductive effects of a primary and secondary alkyl group and is consistent with the ν(CO) trends in the IR spectra.

Scheme I

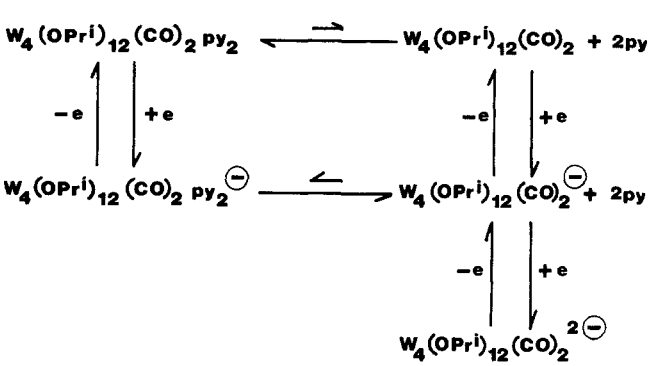

Only one oxidative process shows any reversibility under any conditions, namely, oxidation of $W_2(OCH_2\text{-}t\text{-}Bu)_6(py)_2(\mu$-CO). This lends support to the supposition that oxidized species react by fission of the C–O bond of an alkoxide ligand, whether by a carbonium ion mechanism, or by proton scavaging from an alkyl substituent at the position β to oxygen.

Tetranuclear Compounds. $[W_2(O\text{-}i\text{-}Pr)_6(\mu$-CO)$]_2$ and $[W_2(OCH_2\text{-}t\text{-}Bu)_6(\mu$-CO)$]_2$ each show two successive reversible reductions, separated by ca. 700 mV. Reductive coulometry at potentials just negative of the primary reduction wave established that the primary wave corresponds to a one-electron process. A subsequent cyclic voltammogram was not the same as the initial scan implying that the monoanion is not stable on this time scale. The similarity in peak heights suggests that the second reduction is also a one-electron process. The large separation of these potentials implies that the two dinuclear centers are strongly conjugated to each other. With less electronic connectivity between the dinuclear centers, a much smaller separation, or indeed, a single two-electron reduction might have been expected.[24]

The effect of adding pyridine to $[W_2(O\text{-}i\text{-}Pr)_6(\mu$-CO)$]_2$ to give the Lewis base adduct $[W_2(O\text{-}i\text{-}Pr)_6(py)(\mu$-CO)$]_2$ is best measured in $[(n\text{-}Bu)_4N][BF_4]$/toluene,[25] since a complex dependence on pyridine concentration is apparent in 0.2 M $[(n\text{-}Bu)_4N][BF_4]$/THF. In the toluene electrolyte, addition of excess pyridine causes the primary reduction at −1.61 V to shift to −1.73 V. This shift to more negative potential is consistent with intuition that addition of another donor ligand will increase the negative charge on the metal with a concomitant increase in the energy of metal-based orbitals. The relatively small magnitude of the shift is consistent with the results of our calculations that the LUMO is an energetically isolated, delocalized metal–metal π-bonding orbital that is not of the proper symmetry to interact with the incoming Lewis base donors.

The shift is not apparent in the secondary reductive process, which appears at exactly the same potential as in the absence of pyridine (Table VII), and even in the presence of a large excess of pyridine as shown Figure 15.

(24) Denti, G.; Jones, C. J.; McCleverty, J. A.; Neaves, B. D.; Reynolds, S. J.; Charsley, S. M. In *Some Recent Advances in the Chemistry of Cr, Mo, and W*; Dilworth, J. R., Lappert, M. F., Eds.; RSC Dalton Division: 1983.

(25) Pickett, C. J. *J. Chem. Soc., Chem. Commun.* 1985, 323.

Table VII. Electrochemical Data for $M_2(\mu\text{-CO})$ Containing Compounds of Mo and W

compd	primary electrode potential[a] oxidation	reduction	solv
$Mo_2(O\text{-}t\text{-}Bu)_6(\mu\text{-CO})$	+0.62	−1.32 (0 °C)	THF
$W_2(O\text{-}t\text{-}Bu)_6(\mu\text{-CO})$	+0.22	−2.11 (0 °C)	THF
$Mo_2(OCH_2\text{-}t\text{-}Bu)_6(py)_2(\mu\text{-CO})$	+0.45	−1.70	THF
$W_2(OCH_2\text{-}t\text{-}Bu)_6(py)_2(\mu\text{-CO})$	+0.00 (−50 °C)	−1.91	THF
$Mo_2(O\text{-}i\text{-}Pr)_6(py)_2(\mu\text{-CO})$	+0.07	−1.59 (22 °C)	THF
$[W_2(O\text{-}i\text{-}Pr)_6(\mu\text{-CO})]_2$	+0.49	−1.66, −2.35 (22 °C)	THF
	+0.54	−1.61, −2.19 (22 °C)	toluene[b]
$[W_2(O\text{-}i\text{-}Pr)_6(py)(\mu\text{-CO})]_2$	+0.22	−1.73, −2.19 (22 °C)	toluene[b]
$[W_2(OCH_2\text{-}t\text{-}Bu)_6(\mu\text{-CO})]_2$	+0.78	−1.57, −2.38 (22 °C)	THF
$(C_5H_5)_2Fe$	+0.54 (22 °C)		THF

[a] Electrode potential vs. SCE. Measured in 0.2 M $[n\text{-}Bu_4N][BF_4]$/solvent; scan rate = 200 mV/s. Temperature is indicated in parentheses for reversible processes; otherwise the process is irreversible. For irreversible processes, $E_p/2$ is quoted; for reversible processes, $E_{1/2} = (E_p^{red} - E_p^{ox})/2$ is quoted. [b] Reference 25.

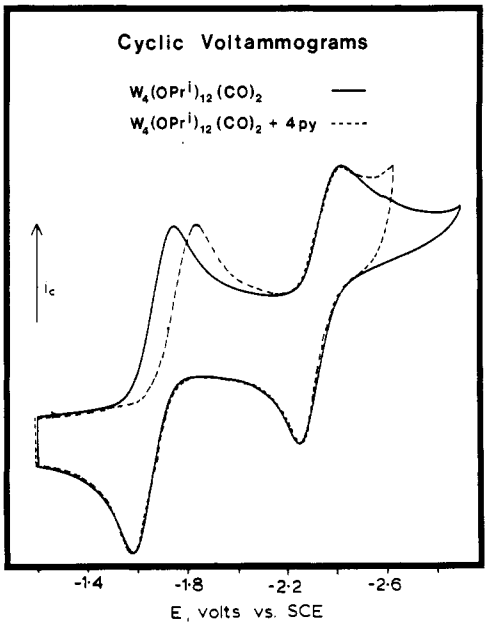

Figure 15. Cyclic voltammograms of $W_4(O\text{-}i\text{-}Pr)_{12}(\mu\text{-CO})_2$ recorded in 0.2 M $[(n\text{-}Bu)_4N][BF_4]$/THF (solid line). After addition of 4 equiv of pyridine (dashed line). Scan rate = 200 mV/s.

This behavior implies that following the initial one-electron reduction, both pyridine ligands are rapidly lost to form the nonligated monoanion $[W_2(O\text{-}i\text{-}Pr)_6(\mu\text{-CO})]_2^-$, according to Scheme I. This observation is also consistent with extensive delocalization of the LUMO between the two $W_2(\mu\text{-CO})$ centers, since otherwise, evidence for a mono-pyridine monoanion might have been anticipated.

In 0.2 M $[(n\text{-}Bu)_4N][BF_4]$/THF the behavior is much more complex. As before, the second reduction is unperturbed by addition of pyridine. The cathodic component of the primary process shifts to more negative potentials depending on the concentrations of added pyridine. The shift in the anodic component, however, is almost unchanged even in the presence of a large excess of pyridine. This reduction is thus rendered irreversible in THF/pyridine. This behavior suggests that the binding of pyridine to $[W_2(O\text{-}i\text{-}Pr)_6(\mu\text{-CO})]_2$ and especially to its monoanion is less favored in THF than in toluene, presumably due to competition from THF ligation. Since THF is usually regarded as a weaker donor relative to pyridine, bonding of THF would be expected to cause smaller negative shifts in $E_{1/2}^{red}$ than binding pyridine.

Quantitative studies of scan-rate dependence in this system, which might have elucidated the mechanism, are rendered difficult by the high specific resistance of the $[(n\text{-}Bu)_4N][BF_4]$/THF systems, leading to significant internal resistance between the working and reference electrodes, and the associated wave distortions with changes in current and scan-rate. Use of more polar solvents was prohibited by the insolubility of the compounds in such media. We are currently constructing new electrodes that will allow us to increase our scan-rate with a view toward resolving this question.

Conclusions

Our calculations suggest that the weakening of the C–O bonds upon interaction with the strongly reducing dinuclear centers can be attributed primarily to the degree of π back-bonding in the $M_2(\mu\text{-CO})$ systems. The differences between Mo and W can be attributed to the combination of relative orbital energies and overlap of Mo 4d vs. W 5d fragment orbitals with CO producing a smaller CO $5\sigma \rightarrow$ metal donation together with a larger metal$\rightarrow$CO 2π back-bonding for tungsten relative to molybdenum systems.[26] Both interactions result in a strengthening of M–C bonding for W- relative to Mo-containing compounds. The comparison of the M–C and C–O bond lengths in Table II indicates that the magnitude of this effect is quite large. A measure of the relative magnitude of π back-bonding can be obtained from the Mulliken populations (or orbital occupancies) of the canonical orbitals of the CO moiety, and a linear correlation exists between the occupation of antibonding carbonyl orbitals and C–O stretching frequencies. Furthermore, we find that π donation from the alkoxide ligands is extremely important. As strong π-donor ligands, the alkoxides serve the important role of enhancing π back-bonding to the μ-CO moiety, and indeed, these $M_2(OR)_6(\mu\text{-CO})$ compounds exhibit the lowest ν(C–O) values of any neutral bridging carbonyl compound in the current literature, and the ν(C–O) values for the $[W_2(OR)_6(\mu\text{-CO})]_2$ compounds are among the lowest (C–O) stretches for compounds with oxygen- and carbon-bound CO.[27] In fact, the bonding of CO in the $[W_2(\mu\text{-CO})]_2$ compounds may serve as a model for the unusual "side-on" binding mode of chemisorbed CO on a Cr(110) surface which shows ν(C–O) in the range 1150–1330 cm^{-1}.[28]

We are encouraged by the self-consistency of all the experimental and theoretical data. The calculations and IR spectral data suggest that W is a better reducing agent

(26) In comparing Mo and W systems in $M(CO)_6$ compounds, Arratia-Perez and co-workers found a greater CO 2π acceptance for W vs. Mo systems as well. See ref 20c.

(27) (a) Horwitz, C. P.; Schriver, D. F. *Adv. Organomet. Chem.* **1984**, *23*, 219 and references therein. (b) Osborne, J. H.; Rheingold, A. L.; Trogler, W. C. *J. Am. Chem. Soc.* **1985**, *107*, 6291 and references therein.

(28) Shinn, N. D.; Madey, T. E. *J. Chem. Phys.* **1985**, *83*, 5928. Side-on bound CO is also reported on a potassium-promoted Ru(001) surface; see: Hoffmann, F. M.; de Poala, R. A. *Phys. Rev. Lett.* **1984**, *52*, 1697.

than Mo, and the electrochemical data also supports this claim. The calculations as well as the spectra indicate that the buildup of negative charge on the carbonyl oxygen is increased for W compounds relative to Mo compounds, and the head-to-tail coupling of $W_2(\mu\text{-CO})$ to $[W_2(\mu\text{-CO})]_2$ compounds is easily rationalized in view of these observations. Thus, these calculations on a series of related compounds have allowed for the correlation of our experimental data, improved our insight into the chemical bonding and reactivity, and stimulated our imagination for future experimentation.

The stepwise reaction involving $W{\equiv}W + C{\equiv}O \rightarrow W_2(\mu\text{-CO})$ followed by $2W_2(\mu\text{-CO}) \rightarrow [W_2(\mu\text{-CO})]_2$ converts $W{\equiv}W$ and $C{\equiv}O$ triple bonds first into double bonds and then into single bonds. Formally the ditungsten center is oxidized $(W{\equiv}W)^{6+} \rightarrow (W{=}W)^{8+} \rightarrow (W{-}W)^{10+}$, and the carbonyl moiety is reduced. This C—O reduction requires the cooperative effects of two ditungsten centers. We believe that the reaction does not stop here, but by further reaction between $(W{\equiv}W)^{6+}$ and $[W_2(\mu\text{-CO})]_2$, the C—O bond of the former carbon monoxide molecule is cleaved to give carbido (C^{4-}) and oxo (O^{2-}) tungsten alkoxide clusters. These matters are currently under investigation. In this regard we note that we have recently observed a facile $C{\equiv}O$ bond cleavage reaction between $(i\text{-PrO})_3W_2(\mu\text{-CSiMe}_3)_2$ and $C{\equiv}O$ leading to the formation of $(i\text{-PrO})_4W(\mu\text{-}\sigma,\pi\text{-CCSiMe}_3)(\mu\text{-CSiMe}_3)W(O\text{-}i\text{-Pr})(=O)$. This represents the first example of the stoichiometric cleavage of $C{\equiv}O$ in a homogeneous reaction at room temperature.[29]

Acknowledgment. We are grateful to the National Science Foundation for financial support. We thank Professor B. E. Bursten of The Ohio State University and Dr. S. Harris of Exxon for helpful discussions. We are also grateful to Professor Bursten for providing copies of the MEDIEVAL, MOPLOT, and CONPLOT programs and instruction on their use. D. L. Clark is the recipient of the 1984-1985 Indiana University SOHIO Fellowship. The VAX 11/780 is an NSF supported departmental facility, CHE-83-09446 and CHE-89-05851.

Registry No. I (M = Mo, R = H), 103671-07-4; I (M = W, R = H), 103671-08-5; I (M = W, R = *t*-Bu), 95674-36-5; I (M = Mo, T = *t*-Bu), 66775-48-2; II (M = W, R = CH_2-*t*-Bu), 95674-37-6; II (M = Mo, R = CH_2-*t*-Bu), 83437-05-2; II (M = Mo, R = Pr-*i*), 83437-00-7; IIIa (R = Pr-*i*), 85956-37-2; IIIb (R = H), 103671-11-0; IIIb (R = CH_2-*t*-Bu), 103692-70-2; IIIb (R = Pr-*i*), 95674-38-7; $Mo_2(OH)_6(NH_3)_2(\mu\text{-CO})$, 103671-09-6; $W_2(OH)_6(NH_3)_2(\mu\text{-CO})$, 103671-10-9.

(29) Chisholm, M. H.; Heppert, J. A.; Huffman, J. C. *J. Chem. Soc., Chem. Commun.* **1985**, 1771.

Organoboranes. 47. An Extremely Facile Elimination of Alkenes from Dialkylhaloboranes. A Comparative Rate Study with Related Trialkylboranes

Herbert C. Brown,* P. V. Ramachandran,[1] and J. Chandrasekharan[2]

Richard B. Wetherill Laboratory, Purdue University, West Lafayette, Indiana 47907

Received April 1, 1986

Dialkylhaloboranes reduce benzaldehyde at a rate much faster than does trialkylboranes. Whereas Ipc_2BCl reduces 2 equiv of benzaldehyde at room temperature almost instantaneously, the related trialkylborane Ipc_2B-*n*-Hex requires approximately 6 days. Sia_2BCl, 2-$MeCpn_2BCl$, Car_2BCl and Ipc_2BBr also reduce benzaldehyde rapidly, but 2-$MeChx_2BCl$ reacts relatively slowly. A cyclic mechanism with a "boat-like" transition state is proposed, which can account for the major differences in the rates of reduction among the various dialkylhaloboranes.

The synthesis of optically active secondary alcohols by the asymmetric reduction of prochiral ketones using chiral organoboron and borohydride reagents has been an active field of study in the recent past.[3] We recently achieved excellent optical yields in the asymmetric reductions of prochiral aromatic ketones with diisopinocampheylchloroborane, Ipc_2BCl (1), readily prepared by the reaction of dry hydrogen chloride in diethyl ether (Et_2O) with diisopinocampheylborane, which in turn is obtained by the hydroboration of α-pinene with BMS.[4] The extremely rapid rate of reduction of ketones by Ipc_2BCl as compared to the trialkylborane *B*-3-pinanyl-9-borabicyclo[3.3.1]nonane, *B*-Ipc-9-BBN [2; Aldrich, Alpine-Borane][5] (eq 1 and 2) attracted our attention, and we undertook a study of the comparative rates of reduction of carbonyls using related dialkylhaloboranes and trialkylboranes.

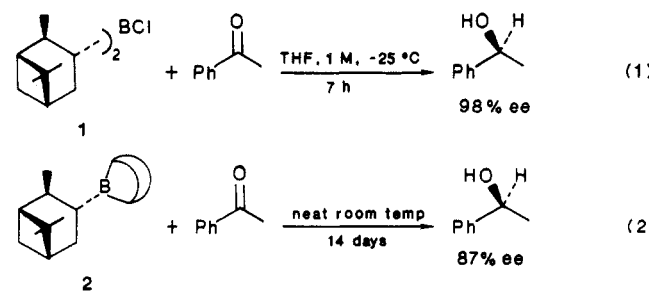

Treatment of Ipc_2BCl (1) with 1 equiv of benzaldehyde at 25 °C resulted in the instantaneous elimination of 1 mol

(1) Postdoctoral research associate on Grant DAAG 850062 from the United States Army Research Office.
(2) Postdoctoral Research Associate on Grant CHE 8414171 from the National Science Foundation.
(3) *Asymmetric Synthesis*; Morrison, J. D., Ed.; Academic Press: New York, 1983; Vol. 2, Chapter 2.
(4) Chandrasekharan, J.; Ramachandran, P. V.; Brown, H. C. *J. Org. Chem.* **1985**, *50*, 5446.
(5) (a) Brown, H. C.; Pai, G. G. *J. Org. Chem.* **1985**, *50*, 1384. (b) Midland, M. M.; Tramontano, A.; Zderic, S. A. *J. Organomet. Chem.* **1978**, *156*, 203.

0276-7333/86/2305-2138$01.50/0